Stem Cell Research & Therapy

RESEARCH

Open Access

Novel pharmaco-exosomal immunotherapy for united airway diseases: PLGA-encapsulated, mesenchymal stem cell-derived exosomes with PPAR-γ agonist for allergic rhinitis and asthma

Khawar Ali Shahzad[1,2†], Zhao Wang[1†], Boyu Cai[1], Xuran Li[1,2], Xiaohui Lv[3], Yanhong Wang[1,2] and Fei Tan[1,2,4,5*]

Abstract

Background The united airway diseases (UADs), exemplified by allergic rhinitis and asthma, cause significant morbidity. Although conventional pharmacotherapy provides symptomatic relief, recent evidence has indicated that cellular therapy, such as stem cell-derived exosomes, might offer therapeutic advantages throughout the entire respiratory tract.

Objectives The present study intends to demonstrate the effect and explore the mechanism of a novel pharmaco-exosomal immunotherapy, i.e., mesenchymal stem cells-derived exosomes (MSC-exo) supplemented with PPAR-γ agonists (Pioglitazone), which is locally delivered using PLGA nanoparticles (PLGA-exo-PIO) for the treatment of allergic airway diseases using male Balb/c mice.

Methods The in vitro and in vivo therapeutic potential was observed using fluorescence imaging, RT-qPCR, ELISA, histopathology, flow cytometry, and bioinformatics analysis.

Results Our results indicated that PLGA NPs exhibited prolonged retention and sustained release in the nasal cavity and lungs. In vitro, PLGA-exo-PIO treatment suppresses LPS-induced inflammation in nasal epithelial cells and mast cells. Using murine models of UADs, PLGA-exo-PIO therapy significantly improved the symptom score, reduced inflammatory cells (i.e., eosinophils and goblets) at tissue levels, and upregulated IFN-γ and IL-10 while downregulating histamine, IgE, LTC4, IL-4, and IL-17. In addition, flow cytometric analysis revealed elevated counts of Th1 cells, Tregs, and Bregs, and reduced Th2 cells, eosinophils, and basophils in the blood and spleen of the treated mice. Finally, the data from bioinformatic analysis supported the therapeutic capabilities of fabricated PLGA-exo-PIO via regulation of multiple signaling pathways, such as the Notch cascade and NF-kB cascade.

†Khawar Ali Shahzad and Zhao Wang are contributed equally as first authors.

*Correspondence:
Fei Tan
iatrologist@163.com

Full list of author information is available at the end of the article

Conclusion For the first time, we used a PLGA-delivered, PIO-strengthened MSC-exo system (PLGA-exo-PIO) as a novel therapy to simultaneously manage AR and asthma as UADs.

Graphical Abstract

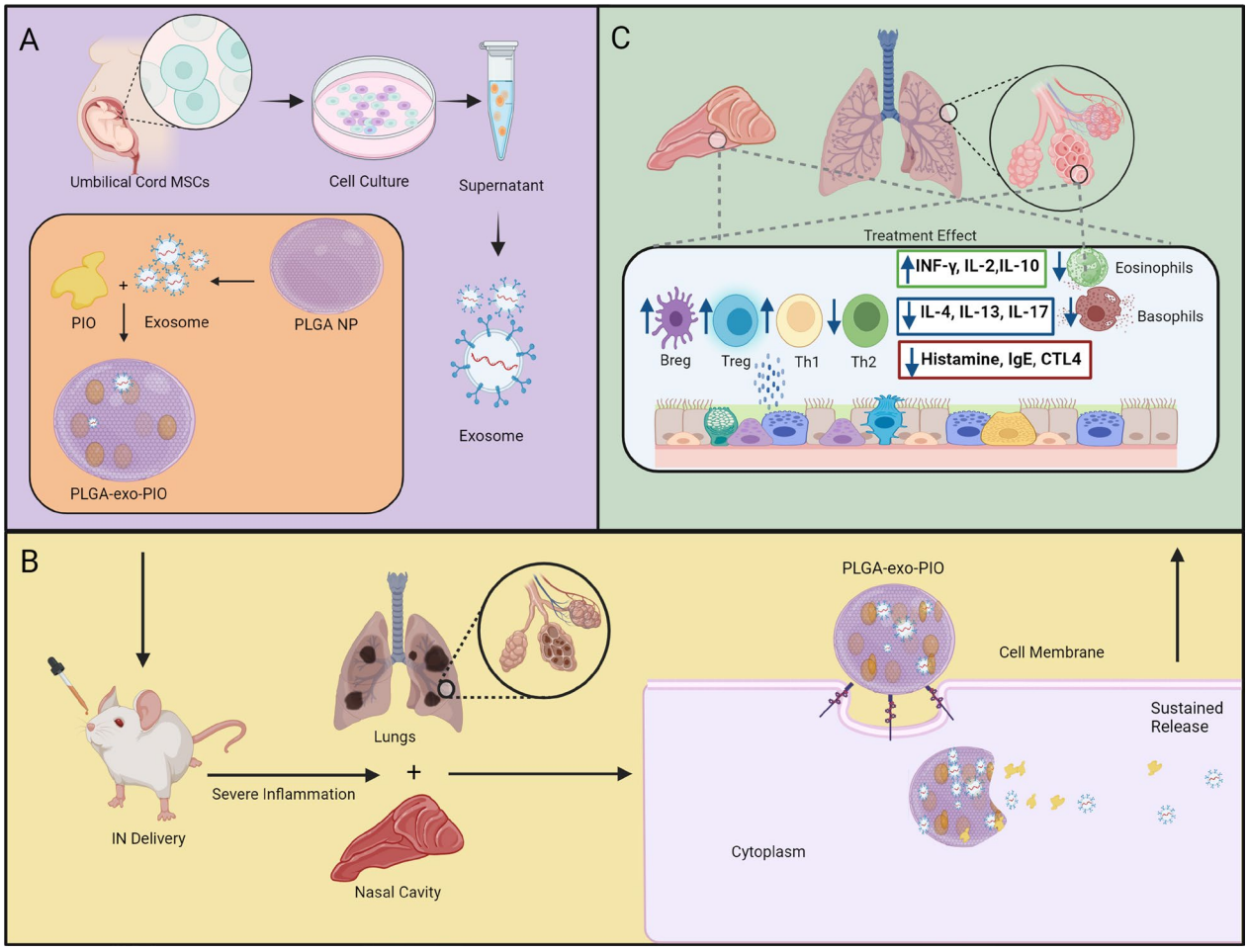

Keywords Allergic rhinitis, Asthma, Exosome, PLGA, Pioglitazone, Notch pathway

Background

The morbidity of allergic rhinitis (AR) and asthma has been steadily increasing over the last several decades, which currently affects approximately 300 million patients worldwide [1, 2]. These two chronic airway inflammatory conditions manifest in the upper and lower airway respectively, resulting in distinctive symptoms and signs while sharing common clinical and immunological basis [3]. In addition, more than two thirds of asthmatic patients have co-existing AR, and treating rhinosinusitis provides improved prognosis for asthma [4]. The morphological and functional connection between the two anatomical units of the same respiratory tract prompted the concept of united airway diseases (UAD) in which AR and asthma share common pathophysiological mechanisms including immunoglobulin E (IgE)-mediated hypersensitivity, T helper (Th) 2 cell-regulated response and elevated eosinophilia [5, 6]. Moreover, some studies also uncovered the presence of Th1 and Th17 signatures in individuals with established severe asthma and concomitant AR [7, 8]. Although conventional pharmacotherapy (e.g. corticosteroids, antihistamines and leukotriene receptor antagonists) could provide symptomatic relief for both upper and lower airway symptoms, none of them is with curative intent or side effects-free [9, 10]. Accumulated evidence has indicated that cellular and biological treatments might offer superior therapeutic advantages to conventional pharmacotherapy.

Stem cell-based therapy has generated tremendous attention as it offers new options for patients suffering from previously incurable diseases. For example, several preclinical and clinical trials adopted the regenerative and

immunomodulatory features of mesenchymal stem cells (MSCs) for the treatment of several respiratory conditions [11]. However, the use of MSCs as therapeutics possesses several drawbacks [12], and exosome, secreted by almost all cell types including stem cells has been posited as a safer and more versatile alternative to stem cell therapy [13]. MSC-derived exosomes (MSC-exo) have been discovered to attenuate inflammation, modulate immune response, inhibit apoptosis, and repair damaged tissues [14, 15]. Although MSC-exo has been used in managing respiratory disorders such as acute respiratory distress syndrome, chronic obstructive pulmonary disease and COVID-19, very scarce evidence is available in airway inflammatory diseases such as AR [16–19] and none in asthma. Nonetheless, exosomes can be engineered, such as drug loading and surface modification, to improve, broaden, or change their therapeutic effects [20]. In our previous study, bioinformatics analysis revealed that exosomes treated nasal mucosal tissues demonstrated peroxisome proliferator-activated receptor (PPAR) signaling pathway to be predominantly activated during exosomal treatment for AR [16], thereby suggesting the potential of using PPAR-γ agonists, such as Pioglitazone (PIO), to further strengthen the anti-inflammatory and immunomodulatory effects of MSC-exos.

Compared to systemic administration, in which exosomes might be rapidly cleared from blood circulation and accumulate in the metabolic organs [21], local delivery of exosomes can improve their organ-specific enrichment, such as intranasal drops for the brain [22] and nebulized inhalation for the lungs [23]. Recently, biomaterials have been used to protect, assist, and augment locally delivered stem cell-derived exosomes to maximize their therapeutic effects [24]. The biomaterials available for exosome delivery are generally characterized according to their composition (e.g., hyaluronic acid, gelatin methacrylate), morphology (e.g., microneedle, nanoparticle), and stimuli-response (e.g., pH, temperature, protein), thereby allowing disease-specific customization [25]. Poly(lactic-co-glycolic acid) (PLGA) has been proven as an excellent carrier of drugs and proteins for the treatment of various diseases because of its outstanding biodegradability and biocompatibility [26, 27]. We recently fabricated a PLGA platform that could efficiently encapsulate and release MSC-exos in the murine nasal cavity in a sustained manner [16]. Specifically, after delineating the in vivo retention time and in vitro exosome release, exosome-encapsulating PLGA nanoparticles (NPs) in 800 nm size with 40 μg/mg exosome cargo were determined to be most suitable for the treatment of allergic respiratory disease and used thereafter.

We are the first group to develop a novel pharmaco-exosomal immunotherapy for united airway diseases. We successfully fabricated PLGA-exo-PIO as an excellent nanoscale drug delivery vehicle with good biocompatibility, longer retention, potent cellular uptake, and targeted therapy to locally deliver the exosomes and PIO for effective treatment of AR and asthma. The results of in vitro and in vivo studies demonstrated that PLGA-exo-PIO exhibits excellent therapeutic capability to attenuate the UADs symptoms by enhancing the anti-inflammatory responses. Further mechanistic exploration of PLGA-exo-PIO treatment revealed multiple signaling pathways such as the Notch cascade and NF-kB cascade.

Methods

Cell culture and mice

We purchased six to eight-week-old male Balb/c mice from Vital River Animal Technology Co., Ltd (Beijing, China), and the mice were housed in specific pathogen free (SPF) conditions and quarantined for one week under standard laboratory conditions (24 °C room temperature, 45%-55% air humidity, and a 12:12 h light/dark cycle). Animal experiments executed in this study were approved by the ethical committee of the School of Medicine, Tongji University, (approval no. TJ-HB-LAL-2024-29) and performed following the recommendations of Guide for Care and Use of Laboratory Animals of the Ministry of Science and Technology of People's Republic of China. The work has been reported in line with the ARRIVE guidelines 2.0.

RBL-2H3 cell line (Cat. # CL-0192) for mast cells and Human nasal epithelial cells (HNEpCs) (Cat. # CP-H252) were obtained from Procell Life Science & Technology, Co., Ltd., (Wuhan, China) and maintained in Minimum Essential Medium (MEM) (Shanghai BasalMedia Technologies, Shanghai, China) supplemented with 15% fetal bovine serum (FBS) (Gibco, Shanghai, China) and 1% penicillin/streptomycin (Gibco, Shanghai, China) at 37 °C in humidified conditions with 95% air and 5% CO_2. Human umbilical cord-derived mesenchymal stem cells (HUC-MSCs) were provided by Cytoniche Biotechnology Co., Ltd., (Beijing, China) and cultured in Dulbecco's Modified Eagle Medium (DMEM) (G4523, Servicebio, China) supplemented with 10% FBS and 1% penicillin/streptomycin (Gibco, Shanghai, China) in humidified conditions with 5% CO_2 and 95% air at 37 °C.

Extraction and purification of MSC-exo

HUC-MSCs derived exosomes (MSC-exo) were extracted from the collected cell culture medium using the ultracentrifugation method as previously described [8, 28] with minor modifications. In brief, HUC-MSCs were cultured in DMEM supplemented with exosome free FBS (A2720-803, Gibco, Shanghai, China). The culture medium was collected when the confluency of the cells reached up to 80%-90%. The cell debris and dead cells from the medium were removed by centrifugation

at 5,000 g for 30 min, followed by the removal of large vacuoles by centrifugation of the medium at 10,000 g for another 30 min. Finally, exosomes were collected by ultracentrifugation (Optima XPN-100 Ultracentrifuge, Beckman Coulter, USA) of culture medium at 120,000 g for 2 h and subsequently washed twice with sterile phosphate buffer saline (PBS) followed by ultracentrifugation again at 120,000 g for 2 h. The pellet was collected as exosomes, resuspended in 100 µL sterile PBS, and stored at -80 °C until use.

The quantification of the exosome concentration was performed using a bicinchoninic acid (BCA) assay kit (Beyotime, Shanghai, China). The size and shape of the extracted exosomes were determined by nanoparticle tracking analysis (NTA) (NS300, NanoSight, Malvern, UK) and transmission electron microscopy (TEM) (FEI F20, Columbus, USA), respectively [29]. Flow cytometric analysis was performed to determine CD9, CD63, and CD81 (BioLegend, USA) markers in the isolated MSC-exo [30, 31].

Fabrication and characterization of blank, ICG-encapsulated, PLGA-exo, PLGA-PIO, and PLGA-exo-PIO nanoparticles

Blank PLGA, indocyanine green (ICG; Macklin, Shanghai, China) encapsulated (ICG-PLGA), exosomes encapsulated PLGA (PLGA-exo), PIO encapsulated PLGA (PLGA-PIO) or exosomes and PIO encapsulated PLGA (PLGA-exo-PIO) were fabricated using double emulsion solvent evaporation method as described by Shahzad et al., [8]. Initially, 100 mg of 0.67 dL/g carboxy-terminated 50:50 PLGA polymer (Macklin, Shanghai, China) was completely dissolved in 5 mL of dichloromethane (Titan Scientific, Shanghai, China) and 20 µL ICG solution (30 mg/mL), exosomes (40 µg/mg PLGA), PIO (200 µg/mg PLGA) or both exosomes and PIO were mixed gently and sonicated for 6 min (10 s sonication and 15 s break) at 90% using an ultrasonic homogenizer (JY92-IIN, Ningbo, Xinzhi, Biotech., Ningbo, China). For blank PLGA nanoparticles (PLGA NPs), nothing was added. The resulting mixture was added to 25 mL 1% poly vinyl alcohol (PVA; Macklin, Shanghai, China) and sonicated again as described previously. Finally, the homogenized solution was added in 50 mL sterile dd H_2O and placed overnight on a magnetic stirrer to evaporate dichloromethane at 4 °C. The solution was then centrifuged in a refrigerated centrifuge machine (Eppendorf, Centrifuge 5810 R, USA) at 6000 RPM for 10 min to collect PLGA NPs. ICG-PLGA NPs were washed twice at 20,000 RPM adding dd H_2O to remove free ICG. ICG-coated exosomes (ICG-exo) were prepared for in vivo tracking analysis by mixing 10 µL ICG in 50 µg exosomes and incubating them in a refrigerator for 12 h. The unattached ICG was removed by ultracentrifugation at 120,000 g for 2 h after adding sterile PBS. The obtained PLGA NPs and ICG-exo were suspended in PBS and stored at -80 °C until further use.

Dynamic light scattering (DLS) (OPT2301140, Opptronic, Shanghai, China) analysis was performed to measure the size and zeta potential of fabricated PLGA NPs. The shape and surface morphology were observed under the scanning electron microscope (SEM) (Hitachi, S-4800, Japan).

In vitro stability, release of exosomes, and loading efficiency of pioglitazone (PIO)

The in vitro release of exosomes from PLGA NPs was estimated by measuring total protein content over time for 10 days. Briefly, 5 mg of PLGA-exo was added to 1 mL PBS in a sterile 1.5 mL Eppendorf tube and mixed thoroughly. The tubes were incubated at 37 °C and 20 µL of the supernatant was replaced with sterile PBS after centrifugation at 10,000 RPM for 10 min every day until day 10. The release profile was measured using BCA assay kit (Beyotime, China). The cumulative release curve was plotted based on the values obtained ($n = 3$).

The amount of PIO entrapped in PLGA NPs was determined using the previously reported indirect method [32]. PLGA-PIO suspension was centrifuged at 10,000 RPM for 10 min in a refrigerated centrifuge machine, and the clear supernatant was collected and concentration of PIO was measured. NanoDrop1000 Spectrometer (ThermoScientific, USA) was used to determine the total percentage of entrapped drug (%EE) at 238 nm.

The stability of the fabricated PLGA NPs was performed by measuring the size and zeta potential using DLS after incubation at 4 °C and 25 °C for 7 days.

Fluorescent imaging for in vivo retention and tissue distribution of PLGA NPs

Fluorescent imaging was performed to evaluate the in vivo retention time and tissue distribution of ICG-PLGA NPs after intranasal (IN), intravenous (IV), and combined (IV + IN) administration. Briefly, 5 mg of ICG-PLGA NPs were suspended in 30 µL (for intranasal) or 100 µL (for intravenous) of PBS and administered through one of the above-mentioned routes in Balb/c mice ($n = 3$). Moreover, 50 µg of ICG-exo suspended on 30 µL of PBS was also administered intranasally in one of the groups. Post-administration fluorescence distribution was evaluated in mice under anesthesia by 3%-5% isoflurane (Shenzhen Reward Life Science and Technology Co., China) mixed with oxygen, at 30 min, 2 h, 6 h, 24 h, 48 h, 72 h, 96 h, and 120 h time points using InVivo Smart-LF system (VISQUE, B12BAA002, Korea) with 1 min exposure time at excitation and emission wavelengths at 740–790 nm and 810–860 nm, respectively. The isoflurane was maintained at 1%-3% once the mice were properly induced and anesthetized. Additionally, at the 2 h time point,

representative mice from each group were sacrificed, and nasal tissues and vital organs (lung, heart, spleen, kidneys, and liver) were imaged to monitor the tissue distribution of ICG-PLGA NPs. The IVIS system was used to analyze the data.

In vitro cellular uptake of PLGA-exo-PIO

HNEpCs and RBL-2H3 cells (1×10^5 cells/well, 500 µL MEM) were seeded in a 12-well 15 mm polystyrene cell culture plate (Nest, USA) for 12 h. The fabricated PLGA-exo-PIO and only exosomes were labeled with PHK26 fluorescent dye (Servicebio, China), and 2 mg of labeled NPs, and 50 µg PHK26 labeled exosomes were cocultured with cells for 4 h, 12 h, 24 h, and 48 h. The cells were then gently washed with cold PBS 3 times, fixed with 4% paraformaldehyde (PFA) (Titan, Shanghai, China) for 15 min at room temperature (RT), and the cell nucleus was stained with DAPI (ThermoFisher, USA). Finally, the pictures were taken using a laser scanning confocal microscope (ECLIPSE Ti2, Nikon, Japan).

Determination of therapeutic effect of PLGA-exo-PIO in vitro

RBL-2H3 cells and HNEpCs (1×10^5 cell/well) were seeded in 12-well cell culture plates adding 500 µL culture medium and allowed to grow overnight. The culture medium was replaced with fresh MEM containing 0.1 µg/mL lipopolysaccharide (LPS) (Sigma-Aldrich, USA) in positive control (LPS) and treatment group (PLGA-exo-PIO), whereas cells without LPS stimulation were considered as negative control (NC) and incubated for 24 h. PLGA-exo-PIO (5 mg/well) was added to the treatment group and incubated again for 24 h. Aseptically collected culture medium from each group was centrifuged at 4000 RPM for 10 min in a refrigerated centrifuge machine, and the supernatant was immediately used for cytokines detection by enzyme-linked immunosorbent assay (ELISA). The collected cells from each group were processed for RNA isolation and real-time quantitative PCR (RT-qPCR) for relative expression of IFN-γ, IL-4, IL-10, and IL-17 in HNEpCs and IL-4 and IL-13 in RBL-2H3 cells. Moreover, the in vitro therapeutic effect of PLGA-exo-PIO treatment was further analyzed by flow cytometry after staining HNEpCs and RBL-2H3 cells.

Establishment of OVA-induced AR and asthma model and their treatment

The OVA-induced AR and airway allergic inflammation (asthma model) was established by following the previously reported method [1]. In brief, all the Balb/c mice except negative control (NC) group were sensitized intraperitoneally injected (i.p) with 200 µL of ovalbumin (OVA) (Sigma-Aldrich, Germany) and aluminum hydroxide ($Al(OH)_3$ (Sigma-Aldrich, Germany) (100 µg OVA + 100 µg ($Al(OH)_3$/100 µL PBS) on day 1, 7 and 14, respectively. The mice were then challenged with 1% OVA solution via IT by nebulization (30 min/day) on days 8, 14, 24, 26, 28, and 30, respectively. The NC group was sensitized and similarly challenged with PBS. AR and asthma signs i.e. number of eosinophils in BALF and symptoms i.e. frequency of scratching and sneezing were recorded and scored for a period of 10 min by blind observers (Fig. S1).

The mice were randomly divided into six groups negative control (NC; normal mice), positive control (PC; AR and asthma mice), blank PLGA treatment (Blank PLGA), PLGA-exo treatment (PLGA-exo), PLGA-PIO treatment (PLGA-PIO), and PLGA-exo-PIO treatment (PLGA-exo-PIO) groups ($n = 12$/group). Six mice of each treatment group were kept in one cage, and each box was tagged with the name of the specified treatment group. All six groups were intranasally administered with specified medications (5 mg/30 µL; 15 µL in each nostril) every 5th day for 6 times. Bronchoalveolar lavage fluid (BALF), lung, spleen, blood, nasal tissues (NT), and other vital organs (liver, kidneys, and heart) were collected 4 days after final treatment by euthanizing the mice of each treatment group by cervical dislocation to minimize the pain.

Collection and analysis of BALF from the lungs

BALF from the euthanized mice of each treatment group was collected following the previously described method [33]. Briefly, 1 mL ice-cold PBS was instilled with a 22-gauge angiocatheter and withdrawn. The process was repeated twice, and the return liquid was collected in a sterile 1.5 mL tube. The collected BALF was centrifuged at 4000 RPM for 10 min at 4 °C and the supernatant was placed at -80 °C until it was used for cytokines analysis. The cell pellet was diluted in 200 µL PBS and stained with Wright-Giemsa (Beyotime, China) stain for total cell, eosinophils and neutrophils count using a modified Neubauer Counter under the light microscope.

Cytokines quantification using ELISA

ELISA was performed to determine the concentrations of histamine (ThermoFisher, USA), IL-4 (Acro Biosystems, USA), and IL-13 (EK213/2 – 01, Multi Sciences, China) cytokines in cell culture supernatant of RBL-2H3 cells, whereas for histamine (LS-F39267, LSBio, USA), IFN-γ, IL-4, IL-10, and IL-17 (GEH0006, GEH0008, GEH0003, GEH0016, Servicebio, China) in HNEpCs by following the manufacturer's protocols. Serum was separated by centrifugation at 5000 RPM for 10 min at 4 °C from collected blood by removing the eyeball of mice with different treatments and examined for histamine (ThermoFisher, USA), IFN-γ (GEM0006, Servicebio, China), IL-4 (88-7044, IL-10 (88-7044, 88-7105, Invitrogen, USA), and

IL-17 (EK217/2 – 01, Multi Sciences, China) as per given protocols. Moreover, the collected BLAF supernatant was used to analyze sIgE (Konodi Bio, China), histamine (ThermoFisher, USA), IFN-γ (GEM0006, Servicebio, China), IL-4, IL-10 (88-7044, 88-7105, Invitrogen, USA), IL-17 (EK217/2 – 01, Multi Sciences, China), and LTC4 (EMCTLA4, Invitrogen, USA) according to the manufacturer's protocols.

Total RNA extraction and RT-qPCR

RNA was extracted using an RNA-Quick Purification Kit (ES Science, China) from spleen tissue and cultured cells (HNEpCs and RBL-2H3) of each treatment group. NanoDrop 1000 spectrometer was used to determine the concentration of total RNA from each sample. 2 μg of extracted RNA was reverse transcribed into cDNA using HiScript cDNA Synthesis Kit (Vazyme, China). RT-qPCR was performed with ABI 7500 Real-Time PCR System (Applied Biosystems, USA) referring to the manufactory's instrument using ChamQ Universal SYBR green based master mix (Vazyme, China). Relative expression of *IFN-γ*, *IL-4*, *IL-10*, and *IL-17* in HNEpCs, *IL-4*, and *IL-13* in RBL-2H3 and *IFN-γ*, *IL-4*, *IL-10*, and *IL-17* in mice was determined using primer sequences given in Supplementary Tables S1, S2 and S3, respectively. Internal calibration was performed using *GAPDH* gene and data were analyzed using the $2^{-\Delta\Delta Ct}$ method.

Histopathology of lung tissue and nasal tissue

Histopathological analysis was performed after collecting the lung and nasal tissues from mice with different treatments. Lung tissues (LT) were fixed for 24 h whereas, nasal tissues for 5 days at RT in 4% paraformaldehyde solution (PFA) (Titan, China). Nasal tissues were then decalcified in EDTA decalcification buffer (Servicebio, China) in a shaking incubator for 3 days at RT. Both tissues were embedded in paraffin after dehydration. Subsequently, hematoxylin and eosin (H&E) and periodic acid Schiff (PAS) staining were performed after cutting the sections of 5 μm using a microtome. Inflammatory infiltration was evaluated in the NT by two blind observers as per reported method [34], whereas eosinophils and goblet cells were calculated by counting cells in 10 different fields at 400× magnification under the light microscope (Nikon, Japan), using Image-Pro Plus software (Media Cybernetics, MD) in stained nasal tissues,

Flow cytometric analysis

Blood and spleens from different treatment groups were processed for lymphocyte separation using lymphocyte separation buffer (BD Biosciences, USA) following the given protocols. Surface staining of the isolated lymphocytes from blood and spleen was performed by adding anti-mouse PE/Cyanine7-CD25, APC-CD4, and FITC-CD19 (BioLegend, USA) antibodies for 30 min at 4 °C. The cells were then fixed for 45 min at 4 °C by fixation buffer (BioLegend, USA) followed by intracellular staining with anti-mouse Brilliant Voilet 421-Foxp3, PE-INF-γ, and Brilliant Violet 605-IL-4 (BioLegend, USA) antibodies for 1 h at 4 °C.

Similarly, after fixation HNEpCs were stained for 1 h at 4 °C with anti-human BV605-IFN-γ, PE/Cy7-IL-4, PE-IL-10, and BV421-IL-17 (BioLegend, USA), whereas RBL-2H3 were stained with anti-mouse PE-IL-13 and Brilliant Violet 605-IL-4 (BioLegend) antibodies.

Additionally, whole blood after removal of red blood cells (RBC) by adding RBCs lysis buffer (P8620, Servicebio, China) was surface stained with anti-mouse PE-CCR3, APC-FcεRI, and FITC-CD63 for 30 min at 4 °C for eosinophils and basophils detection in blood. Moreover, the collected cells from BALF were surface stained for 30 min at 4 °C with anti-mouse FITC-CD170, APC-CD45, and PE-CD11c antibodies to detect eosinophils. Ultimately, flow cytometric analysis was performed on LSRFortessa Cell Analyzer (BD, Biosciences, USA), and the data were analyzed by FlowJo 10.8.1 software.

Transcriptomic data acquisition and trend analysis

The nasal mucosa tissues and lung tissues of AR and asthma model mice were isolated and used for RNA sequencing ($n = 3$ in each group). RNA library preparation, sequencing, and analysis were performed by 10 K Genomics (Shanghai, China). In brief, messenger RNA was purified from total RNA using poly-T oligo-attached magnetic beads. The first strand cDNA was synthesized using random hexamer primers followed by the second strand cDNA synthesis, and the library was checked with Qubit and real-time PCR for quantification. After the library QC, it is pooled according to the effective concentration and the target data output required for the experiment, then subjected to Illumina sequencing, which produces 150 bp paired-end reads. Paired-end clean reads were aligned to the reference genome using Hisat2 v2.0.5, and FeatureCounts v1.5.0-p3 was used to count the reads numbers mapped to each gene.

The heatmap was plotted using the SRplot tools (https://www.bioinformatics.com.cn), an online platform for data analysis and visualization. Venn diagram is visualized using the 'ggvenn' package in R software (version 4.3.0). To understand the potential functions of the consistently upregulated genes in the PLGA-exo-PIO group or the PC group, we performed Gene Ontology (GO) term annotation, and the results were visualized using OmicShare tools (https://www.omicshare.com/tools). The 'cnetplot' function and the 'treeplot' function from the 'enrichplot' package were used to draw the GO term network and the tree diagram.

Enrichment analysis of differentially expressed genes

Differentially expressed genes (DEGs) were screened using the 'edgeR' package with the screening criteria: $p < 0.05$ and $|FC| \geq 2.0$. Data were submitted to the 'ggplot2' package to construct the volcano plots. The OmicShare tool was further used to analyze the KEGG enrichment pathways of the DEGs. Gene Set Enrichment Analysis (GSEA) was performed using the 'gseGO' function in the 'clusterProfiler' package. The enrichment results were visualized using the 'dotplot' function and the 'gseaplot2' function in the 'enrichplot' package (p value < 0.05, p.adjust < 0.25).

Organ toxicity evaluation

Peripheral blood and vital organs (kidney, liver, spleen, and heart) were collected from mice of different treatment groups, 24 h after the final administration. Routine blood and serum tests were performed to evaluate the liver and kidney functions by an automated biochemistry analyzer (Siemens Healthcare Diagnostics Inc, Germany). At the same time, the vital organs were fixed in 4% paraformaldehyde, embedded in paraffin, and sections were processed for H&E staining.

Statistical analysis

All the data were statistically analyzed, and figures were generated using GraphPad Prism (version 9.5) software (GraphPad, USA). The measured parameters are presented as mean ± standard deviation (SD). The group mean values were analyzed by one-way analysis of variance (ANOVA) and then by Tukey's test for multiple comparisons. The difference between the two independent groups was determined by student's t-test. The experiments for exosomes and PLGA characterization were performed in triplicate. The experiments for in vitro studies were performed with $n = 3$, whereas for in vivo studies $n = 6$ for each treatment group. We analyzed and calculated the fluorescence intensity of PHK-26 at each time point using the ImageJ software. p values less than 0.05 were considered statistically significant, indicated as $^{*}p < 0.05$; $^{**}p < 0.01$; and $^{***}p < 0.001$.

Results

MSC-exo were successfully extracted and identified, and PLGA encapsulation of exosomes with and without PIO was characterized using various parameters

The isolated vesicles with an average diameter between 30 and 150 nm were identified using NTA analysis (Fig. 1A and B). A double-layered membrane and cup-shaped morphology were observed under the transmission electron microscope (Fig. 1C). The purified exosomes were positive for CD9, CD63, and CD81 markers when flow cytometric analysis was performed, indicating successful isolation of MSC-exo (Fig. 1D). The mean protein concentration of isolated and identified exosomes was determined to be 48.5 ± 2.43 μg/μL and 3.2×10^8 particles/mL using the nanodrop and NTA assay, respectively.

The fabricated PLGA NPs exhibited a spherical shape and smooth surface morphology (Fig. 1E). Size and zeta potential analysis by DLS showed 788.5 ± 13.29 nm, 814.6 ± 6.38 nm, and 807.1 ± 4.01 nm size in diameter and − 11.7 ± 2.89 mV, -17.0 ± 3.01 mV and − 12.7 ± 4.59 mV zeta potential for blank PLGA, PLGA-PIO and PLGA-exo-PIO, respectively (Fig. 1F and G). ICG-PLGA with an average diameter of 806.5 ± 9.02 nm and − 15.3 ± 1.93 mV zeta potential presenting green fluorescence were fabricated (data not shown). The in vitro release kinetics of PLGA-exo was investigated using a BCA quantification assay. PLGA-exo exhibited a sustained release profile as 90% of the encapsulated exosomes were released at day 9 (Fig. 1H). Post-release NTA and flow cytometric analysis demonstrated the structural integrity of exosomes by detecting the size and exosomal marker proteins after release from PLGA nanoparticles (Fig. S3A & B). DLS analysis for exosome size before and after sonification demonstrated no significant change, indicating short-time sonification did not affect the stability of the exosomes (Fig. S2). The results of drug loading efficiency showed that 69.6% of the total PIO was loaded in PLGA NPs, whereas UV spectrometry indicated that 90% of PIO was released from PLGA after 9 days in parallel to exosomes (Fig. 1I and J). Flow cytometry and NTA analysis revealed that exosomes remain intact after being released from PLGA nanoparticles and retain their functional cargo (proteins) (Fig. S3). Finally, the fabricated PLGA NPs were found stable at 4 °C with non-significant change in size and zeta potential, whereas the size and zeta potential were significantly changed after day 3 at 25 °C (Fig. 1K and L).

PLGA NPs exhibited sustained release in the nasal cavity and lungs, with intranasal delivery being a superior modality to intravenous administration

The retention time and suitable route of drug delivery were determined by comparing intranasal (IN), intravenous (IV), and combined (IN + IV) administration of ICG-PLGA in Balb/c mice followed by in vivo and ex vivo fluorescence imaging. The whole-body fluorescence imaging (IVIS) demonstrated that ICG-PLGA reached the targeted organs, i.e., nasal tissue (NT) and lung tissue (LT), 30 min after the IN and IV + IN administration. Strong fluorescence in NT and LT was observed after 24 h in IN group, whereas 12 h in the IN + IV route. However, the retention time for both routes were almost the same (120 h) (Fig. 2A). On the other hand, IV administration of ICG-PLGA resulted in rapid clearance with no fluorescence in targeted organs after 6 h as indicated by the third panel of Fig. 2A. However, IN delivery of ICG-exo

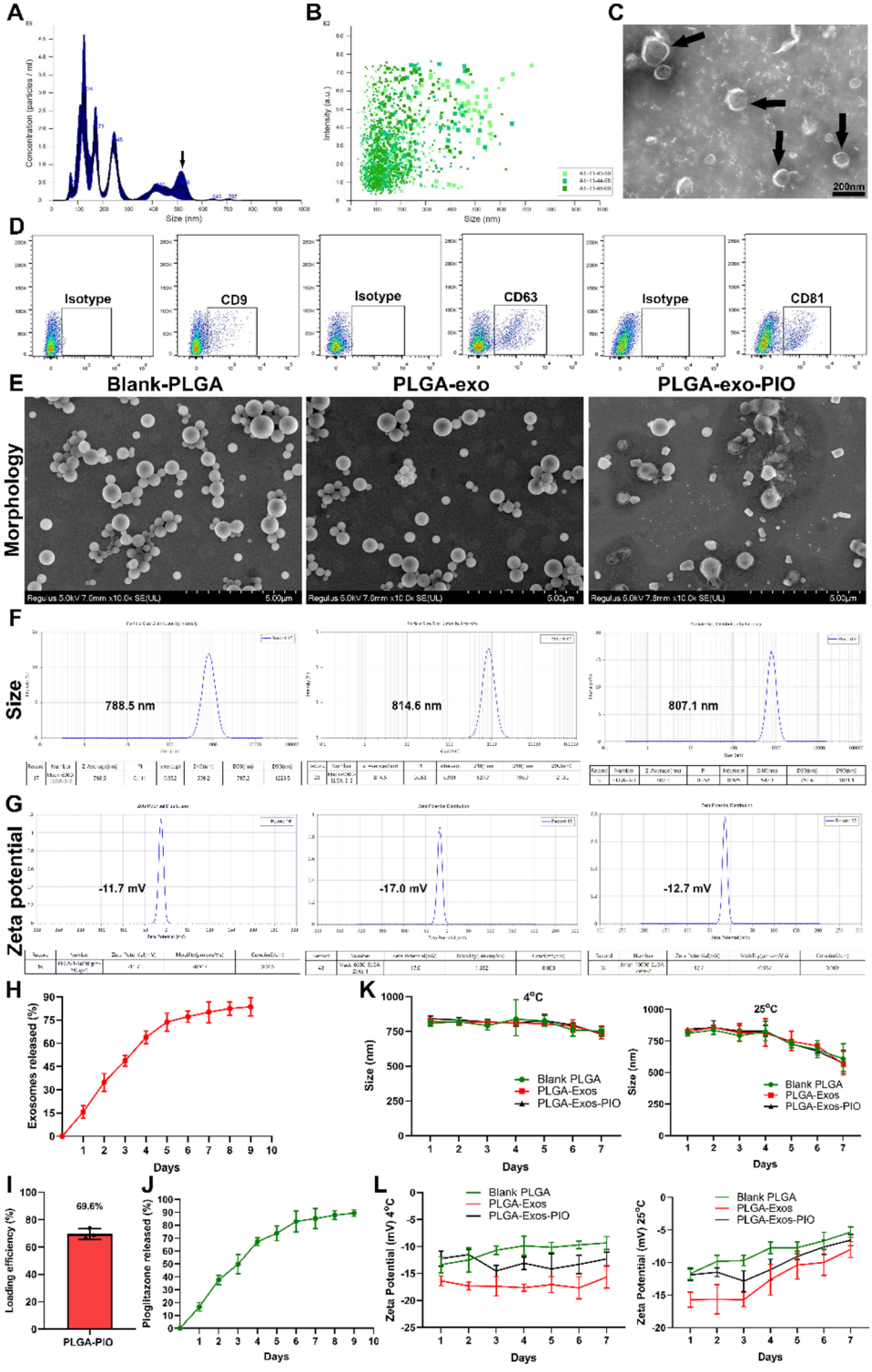

Fig. 1 Characterization of MSC-exosomes, and fabricated PLGA-exo-PIO. (**A-B**) Size distribution of MSC-exosomes by NTA analysis. (↓) the peak indicating the clustering of exosomes during analysis. (**C**) TEM image of MSC-exosomes; scale bar 200 nm. (**D**) Representative dot plots of exosomes for CD9, CD63, and CD81 surface markers. (**E**) Representative SEM micrographs; scale bar 5 µm. (**F**) Size distribution, and (**G**) zeta potential analysis of blank PLGA, PLGA-exo, and PLGA-exo-PIO. (**H**) Quantitative release analysis of exosomes from PLGA NPs over time. (**I**) Loading efficiency of PIO in PLGA NPs. (**J**) Quantitative release analysis of PIO from PLGA NPs over time. (**K-L**) Stability evaluation by size and zeta potential analysis for fabricated blank PLGA, PLGA-exo, and PLGA-exo-PIO at 4 °C and 25 °C. Data are presented as mean ± SD (performed in triplicate; $n = 3$ in each group)

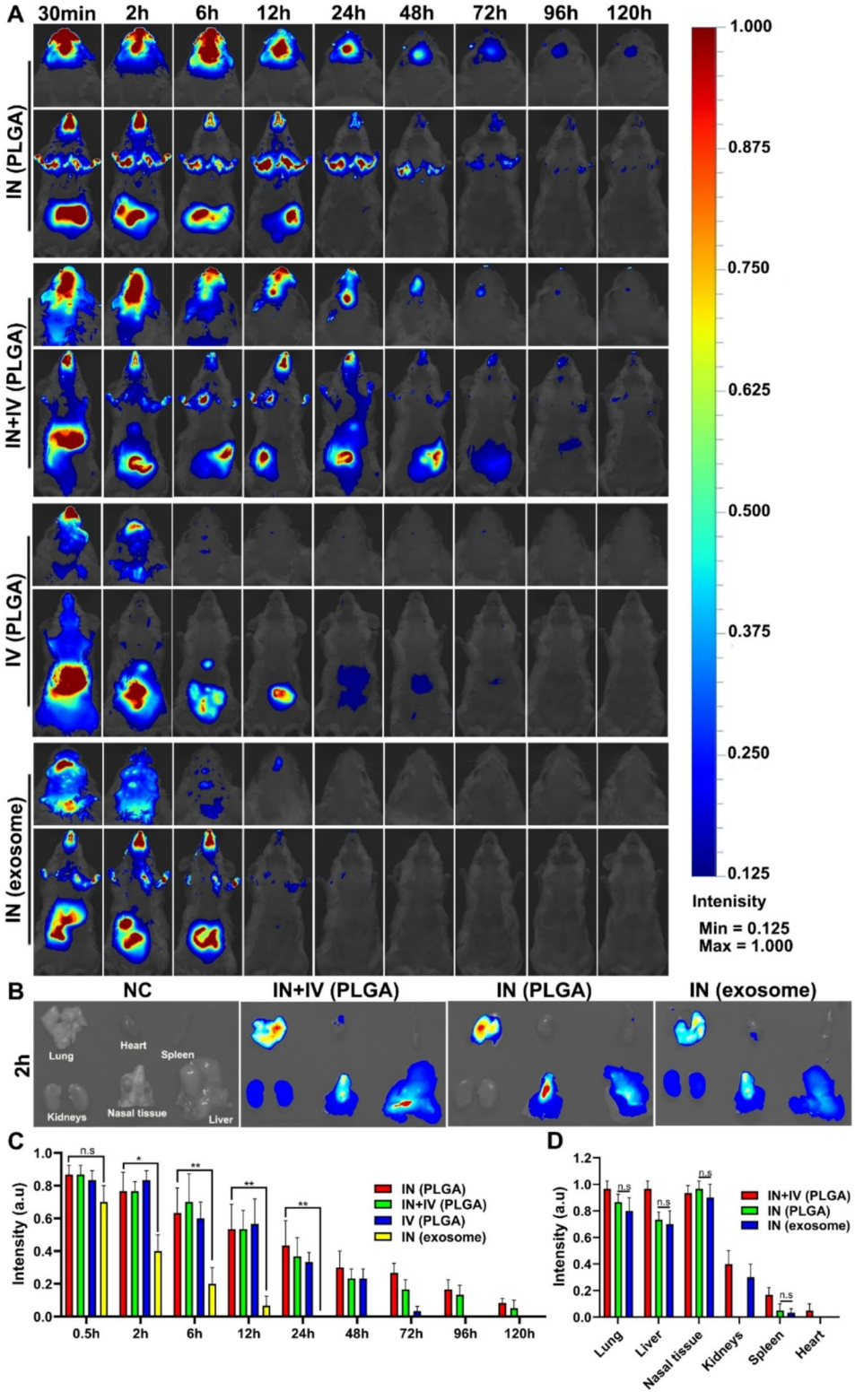

Fig. 2 In vivo tracking and biodistribution of PLGA NPs and exosomes. (**A**) The whole body and the head portion of Balb/c mice were imaged by near-infrared fluorescence imaging at different time points after intranasal, intravenous, and combined (intranasal and intravenous) administration of ICG-PLGA and intranasal inoculation of ICG-exo. (**B**) Ex vivo accumulation of ICG-PLGA and ICG-exo after administration by different routes at 2 h time point in excised vital organs. (**C**) The signal intensity in different groups at different time points. (**D**) The signal intensity in different organs at 2 h time point. Data are presented as mean ± SD ($n = 3$ in each group, n.s = not significant, $^{*}p < 0.05$, $^{**}p < 0.01$)

demonstrated complete disappearance of fluorescence after 24 h (panel four, Fig. 2A). The ex vivo imaging of excised vital organs indicated that ICG-PLGA and ICG-exo were mainly accumulated in nasal tissue, lungs, liver, kidneys, and heart by IN + IV and IN delivery, whereas IN delivery of ICG-PLGA showed no fluorescence in heart and kidneys (Fig. 2B). The fluorescence intensity of each time point for in vivo imaging and ex vivo imaging at 2 h was also measured and quantified (Fig. 2C and D). Therefore, IN route of PLGA-exo-PIO delivery was chosen in further in vivo experiments.

PHK26-labelled PLGA-exo-PIO and exosomes were used as fluorescent indicators to monitor the internalization of PLGA-exo-PIO and exosomes. Our data showed that PLGA-exo-PIO were gradually internalized in HNEpCs and RBL-2H3 cells, and maximum fluorescence was observed at 24 h in both cell lines (Fig. 3A and B, S4A). However, rapid internalization of PHK26-exo with strong red fluorescence was observed at 12 h followed by the quick clearance in HNEpCs (Fig. S4B). These results signify the importance of PLGA NPs as efficient carriers to deliver exosomes and PIO in nasal epithelial and mast cells.

PLGA-exo-PIO treatment suppresses LPS-induced inflammation in vitro

The therapeutic potential of PLGA-exo-PIO was evaluated by treating LPS-stimulated HNEpCs and RBL-2H3 cells as an in vitro AR + asthma model. qPCR and ELISA analysis determined the levels of mRNA and cytokines. As shown in Fig. 3C, the levels of IFN-γ, and IL-10 were decreased, whereas IL-4 and IL-17 were increased after LPS stimulation in HNEpCs. Treatment with PLGA-exo-PIO significantly the upregulated the expression levels of mRNA for *IFN-γ*, and *IL-17*, whereas *IL-4* and *IL-17* were downregulated significantly compared with the positive control (LPS) group in HNEpCs. Likewise, the levels of the histamine, IL-4, and IL-17 cytokines were decreased whereas IFN-γ and IL-10 levels were decreased (Fig. 3D) in the supernatant. Additionally, the flow cytometry results also validated the ELISA and TR-qPCR analysis as the treatment group exhibited higher IFN-γ and IL-10 whereas lower IL-4 and IL-17 positive cells compared with the LPS group (Fig. 3E and H).

Similarly, as depicted in Fig. 3I and J, LPS-stimulated mast cells also exhibited a higher percentage of cells with Th2-related (IL-4 and IL-13) markers, however, a significant reduction in their population was observed in the PLGA-exo-PIO treatment group. In addition, histamine and Th2-related cytokines (IL-4 and IL-13) were also significantly reduced after PLGA-exo-PIO treatment (Fig. 3K). The same trend was observed for IL-4 and IL-13 mRNA expression (Fig. 3L). These results suggested that PLGA-exo-PIO treatment can exert an anti-inflammatory effect by regulating the Th1/Th2 balance and downregulating histamine production.

PLGA-exo-PIO treatment markedly depletes the inflammatory cells and factors in OVA-induced AR and asthma mice model

To examine the in vivo treatment effect of PLGA-exo-PIO, the frequency of scratching and sneezing, and the number of eosinophils in BALF of the AR + asthma mice were recorded. The results showed that PLGA-exo-PIO treatment significantly reduced the number of scratching and sneezing in AR + asthma mice (Fig. 4A). Moreover, the eosinophils count in BALF was also reduced in AR + asthma mice (Fig. 4B). In response to the OVA challenge, the levels of histamine, total IgE and LTC4 in the serum of PC group were increased to 12.43 ± 2.31 ng/mL, 17.64 ± 5.82 ng/mL, and 9.87 ± 1.65 ng/mL, respectively, and reduced to 6.35 ± 1.18 ng/mL, 4.75 ± 3.71 ng/mL, and 2.65 ± 1.80 ng/mL, respectively, after PLGA-exo-PIO treatment (Fig. 4C). Additionally, results of RNA sequencing demonstrated that the genes related to cilium organization and microtubule bundle formation were upregulated, and the genes involved in immunoglobulin-mediated immune response and cytokine-mediated signaling pathway were downregulated in treated nasal and lung tissues (Fig. 5C and D). When compared with PC and blank PLGA groups, AR + asthma mice treated with PLGA-PIO, PLGA-exo, and PLGA-exo-PIO, as indicated by H&E and PAS staining results, showed a significantly less infiltration of inflammatory cells in lungs with lower peri-bronchial infiltrates and goblet cells hyperplasia (Fig. 4D). The thickness of the nasal mucosa and infiltration of eosinophils in PC group (44.5 ± 9.75) was significantly higher than that of NC group (5 ± 2.75). However, the thickness and extent of eosinophils infiltration were significantly reduced ($p < 0.01$) in PLGA-PIO (30.65 ± 6.25), PLGA-exo (19.25 ± 2.95), and PLGA-exo-PIO (9.98 ± 1.89) groups. The PC group had significantly increased goblet cell hyperplasia (39.25 ± 10.48). However, PLGA-exo-PIO treatment has a better effect than exosome or PIO alone in suppressing the goblet cell proliferation in nasal mucosa (Fig. 4E). Furthermore, we collected nasal mucosa and lung tissues from the PC and PLGA-exo-PIO groups for RNA sequencing. Sequencing analysis revealed that the inflammation-related signaling pathways including, leukocyte migration signaling pathway, TNF signaling pathway, NF-kappa B signaling pathway and IL-17 signaling pathway were decreased after PLGA-exo-PIO treatment (Fig. 6C and D). The detailed elaboration of RNA sequencing results is in the bioinformatics results section.

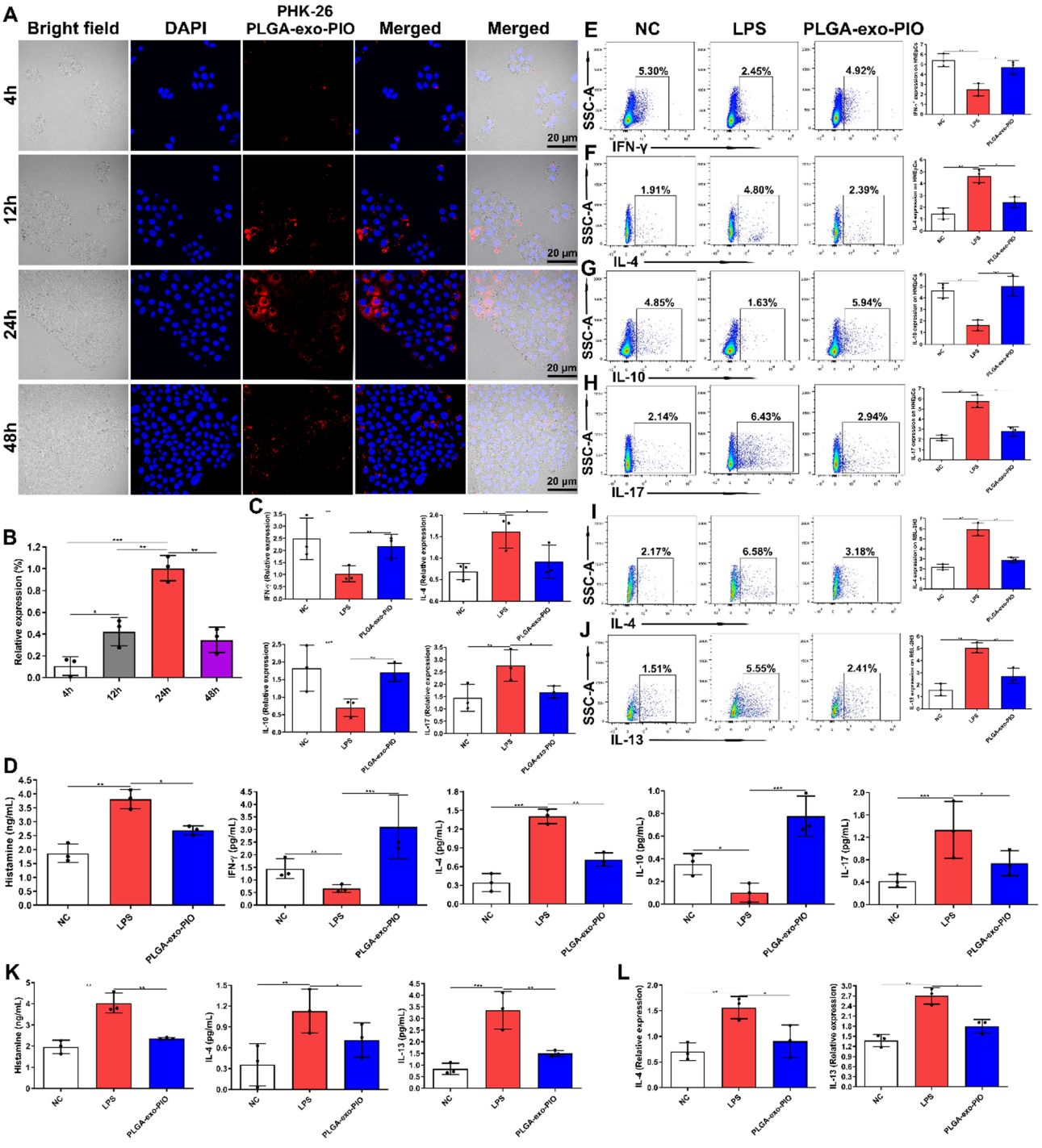

Fig. 3 In vitro cellular uptake and treatment effect of PLGA-exo-PIO. (**A**) Representative confocal microscopy images presenting internalization of PLGA-exo-PIO in HNEpCs at different time points; scale bar 20 μm. (**B**) The statistical data of fluorescence intensity at each time points (**C**) Relative expression of mRNA for IFN-γ, IL-4, IL-10, and IL-17 in HNEpCs, determined by RT-qPCR. (**D**) The concentrations of histamine, IFN-γ, IL-4, IL-10, and IL-17 in HNEpCs, determined by ELISA. The frequencies of (**E**) IFN$^+$ (**F**) IL-4$^+$ (**G**) IL-10$^+$, and (**H**) IL-17$^+$ HNEpCs after treatment. The frequencies of (I) IL-4$^+$, and (**J**) IL-13$^+$ RBL-2H3 cells after treatment. (**K**) The concentrations of histamine, IL-4, and IL-13 in RBL-2H3 cells, determined by ELISA. (**L**) Relative expression of mRNA for IL-4, and IL-13, in RBL-2H3 cells, determined by RT-qPCR. ($n = 3$ in each group, *$p < 0.05$, **$p < 0.01$, ***$p < 0.001$)

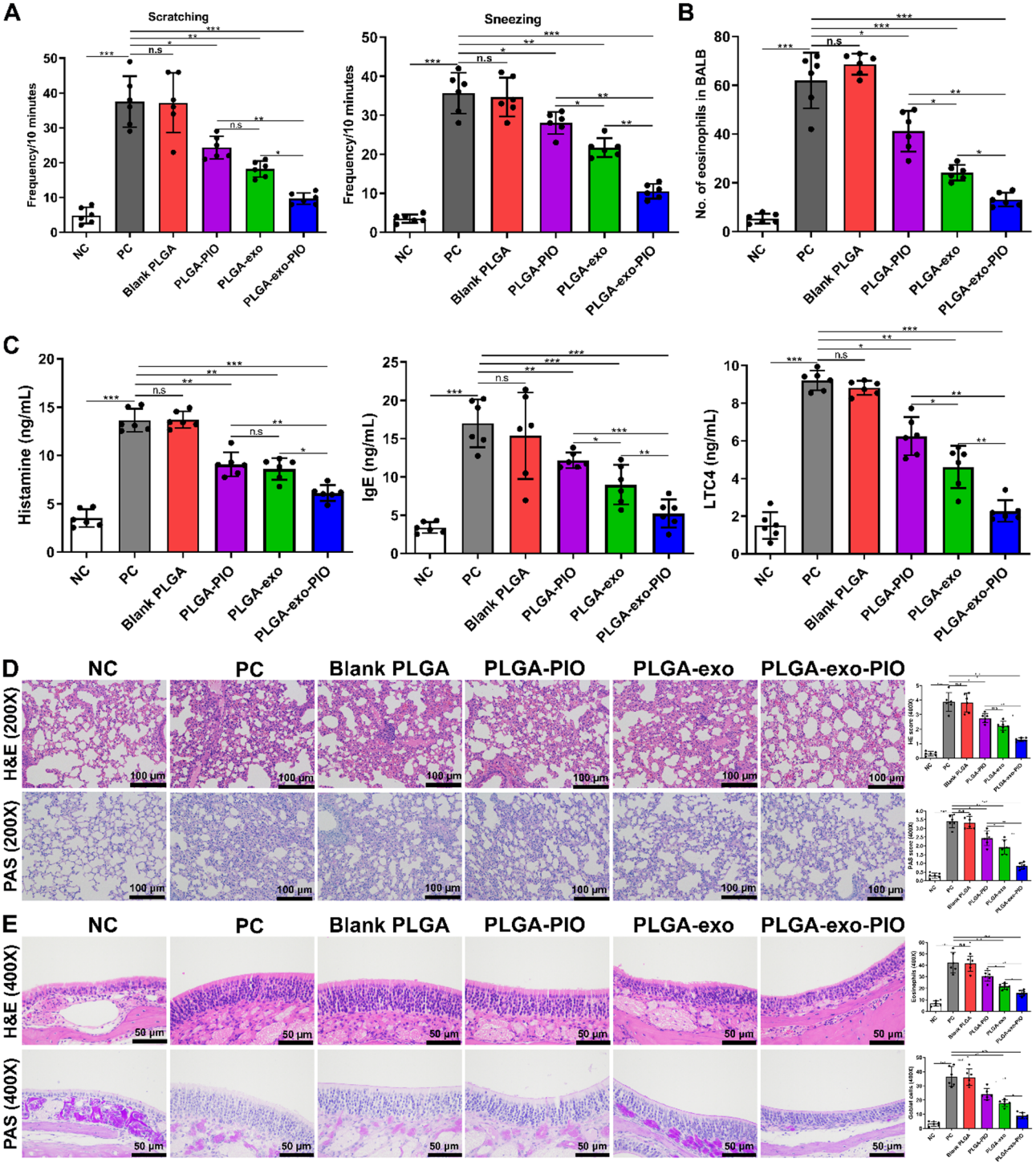

Fig. 4 Assessment of therapeutic effect by intranasal administration of PLGA-exo-PIO in AR + asthma mice. (**A**) Frequency of scratching and sneezing, and (**B**) number of eosinophils in BALF after treatment. (**C**) The concentrations of histamine, IgE, and LTC4 in the serum. (**D**) Representative H&E and PAS images of lungs from mice after treatment; scale bar 100 μm (200X). (**E**) Representative H&E and PAS images of nasal tissues from mice after treatment; scale bar 50 μm (400X). ($n = 6$ in each group, $^{*}p < 0.05$, $^{**}p < 0.01$, $^{***}p < 0.001$)

PLGA-exo-PIO treatment regulates the expression of pro- and anti-inflammatory genes and attenuates inflammatory infiltration in the spleen of AR and asthma mice

Next, we determined whether PLGA-exo-PIO treatment could regulate the expression of Th1, Th2, IL-10, and IL-17-related mRNA in vivo. After final dose, total RNA was extracted from the spleen, and *IFN-γ*, *IL-4*, *IL-10*, and *IL-17* gene expression was detected. As shown in

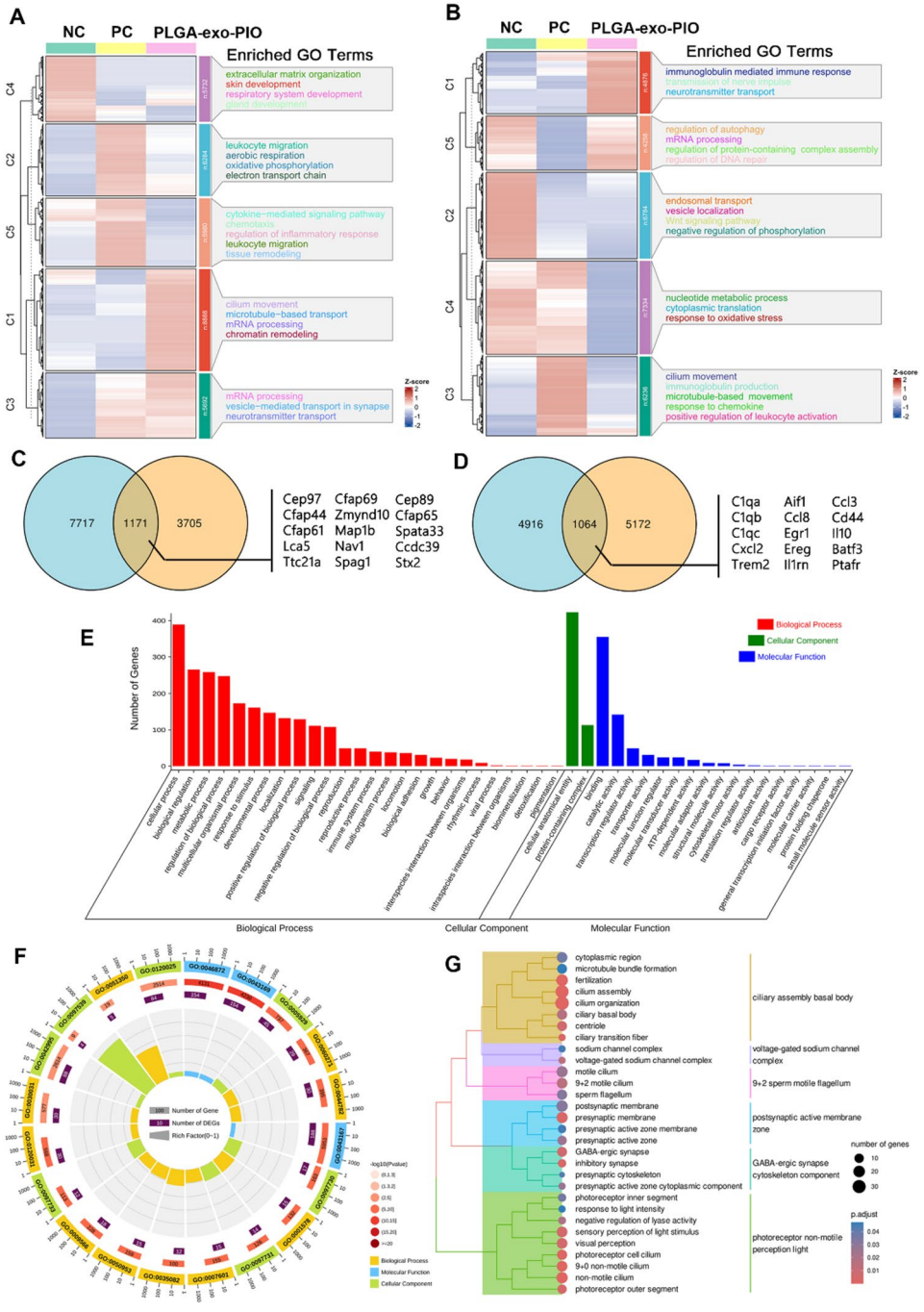

Fig. 5 Trend analysis shows consistent functional changes in AR and asthma. (**A, B**) Heatmap and hierarchical clustering of genes involved in the NC, PC, and PLGA-exo-PIO groups in NT (**A**) and LT (**B**). The colors represent the relative gene expression values after normalization adjustments. (**C**) Venn analysis of upregulated genes in the PLGA-exo-PIO group based on C1 genes in NT and C1 genes in LT. (**D**) Venn analysis of upregulated genes in the PC group based on C5 genes in NT and C3 genes in LT. (**E**) The consistently upregulated genes after treatment were selected to do enrichment tests to reveal the enrichment of GO terms. Statistically significant molecular functions, biological processes, and cellular components were identified. Each color block represents the gene amount in each tissue. (**F**) A GO enrichment of the consistently upregulated genes and twenty significantly enriched GO terms are shown. (**G**) The tree diagram shows the hierarchical clustering of enriched GO terms

Fig. 7A, IFN-γ, and IL-10 expressions were significantly upregulated, whereas IL-4 and IL-17 were downregulated after treatment with PLGA-exo-PIO. In parallel, lymphocytes isolated from the spleen were stained for flow cytometry to further validate the effect of PLGA-exo-PIO therapy on Th1, Th2, Treg and Breg cells. Our results indicated that Th1 cells, Tregs, and regulatory B cells (Bregs), were significantly decreased, and Th2 cells were

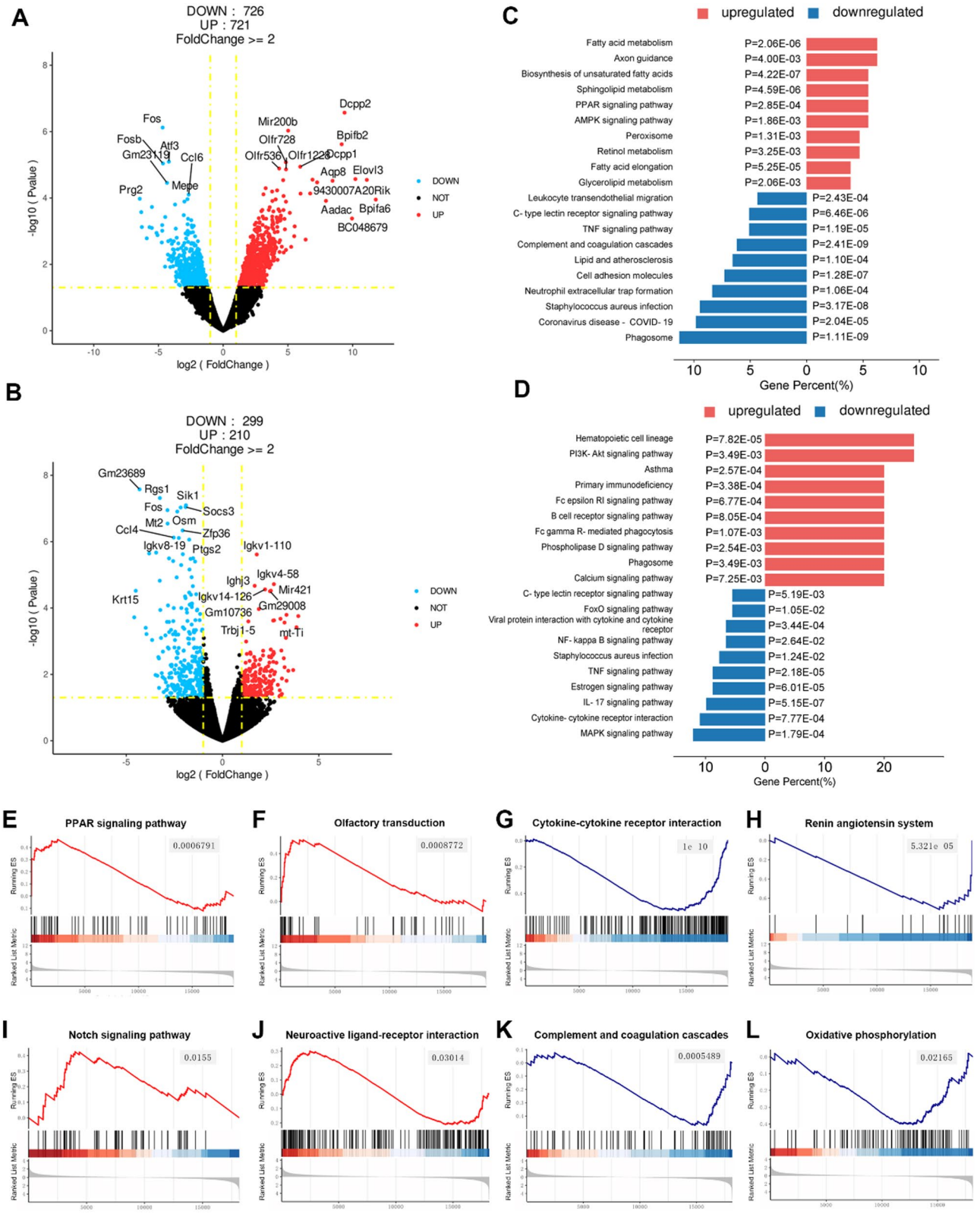

Fig. 6 (See legend on next page.)

(See figure on previous page.)

Fig. 6 Signaling pathways of PLGA-exo-PIO for the treatment of AR and asthma. (**A, B**) The volcano plots of NT (**A**) and LT (**B**) by comparing the gene expression abundance between the PC and the PLGA-exo-PIO group. The logarithmic fold changes of gene expression were plotted by the negative decadic logarithm of the *p*-value. The red genes are upregulated and the blue genes are downregulated. |log2 (FC)| >1 is considered to be significant. (**C, D**) Selected enrichment results of KEGG pathways in the PLGA-exo-PIO versus PC group in NT (**C**) and LT (**D**). (**E-H**) In NT, GSEA enrichment plots of the PLGA-exo-PIO group were compared with the PC group for the PPAR signaling pathway (**E**), olfactory transduction (**F**), cytokine-cytokine receptor interaction (**G**), and renin angiotensin system (**H**). (**I-L**) In LT, GSEA enrichment plots of the PLGA-exo-PIO group were compared with the PC group for the notch signaling pathway (**I**), neuroactive ligand-receptor interaction (**J**), complement and coagulation cascades (**K**), and oxidative phosphorylation (**L**)

significantly increased in OVA-induced AR + asthma mice. The frequencies of Th1 ($CD4^+IFN\text{-}\gamma^+$) cells were 3.62 ± 1.57, 2.19 ± 0.65, 2.46 ± 4.17, 4.1 ± 1.73, 7.62 ± 3.87, and 12.3 ± 2.79, in NC, PC, Blank PLGA, PLGA-PIO, PLGA-exo and PLGA-exo-PIO groups, respectively, after 6 doses of treatment (Fig. 7B). When compared with the PC group, the PLGA-exo-PIO treatment led to 83.6% of the frequency of Tregs in the spleen, while PLGA-exo and PLGA-PIO resulted in a 71.9% and 62.3% increase, respectively (Fig. 7C). Similarly, the population of Bregs decreased to 2.26 ± 1.31 in PC group but increased to 4.65 ± 1.14, 5.41 ± 2.19, and 8.24 ± 2.56 in PLGA-PIO, PLGA-exo, and PLGA-exo-PIO groups, respectively, after final dose. Conversely, the mean percentage of $CD4^+IL\text{-}4^+$ Th2 cells was increased to 6.36 ± 2.74 and 6.12 ± 2.48 in PC and Blank PLGA groups whereas decreased to 5.80 ± 1.94, 4.07 ± 0.86, and 1.63 ± 0.57 in PLGA-PIO, PLGA-exo, and PLGA-exo-PIO treatment groups, respectively (Fig. 7D). The results of flow cytometric analysis for Bregs are illustrated in Fig. 7E. These data suggest that PLGA-exo-PIO are capable to attenuate the chronic united airway diseases.

PLGA-exo-PIO treatment reduces the inflammatory cells and cytokines in the blood of AR and asthma mice

It is well known that Th1/Th2 cells, their effector cytokines, infiltration of eosinophils, and degranulation basophils all play an important role in the pathophysiology of chronic inflammatory respiratory disorders. Levels of Th1-associated cytokine IFN-γ, Th2-associated cytokine IL-4, Th17-associated IL-17, and IL-10 were examined in serum to elucidate the effect of PLGA-exo-PIO on Th1/Th2/Th17 responses. The ELISA results showed that the levels of IFN-γ and IL-10 cytokines were significantly increased, whereas IL-4 and IL-17 decreased in the serum of AR + asthma mice that were treated with PLGA-exo-PIO when compared to the positive control (PC) (Fig. 8A). Moreover, PBMCs collected from the blood of different treatment groups were processed to assess the frequencies of Th1, Th2, Treg and Breg cells using flow cytometry. The frequencies of $IFN\text{-}\gamma^+CD4^+$ T cells, Tregs, and Bregs were decreased, whereas $IL\text{-}4^+CD4^+$ T cells were increased in OVA-induced mice demonstrating the development of inflammatory responses. As presented in representative dot plots Fig. 8B and D, the populations of $IFN\text{-}\gamma^+CD4^+$ T cells, Tregs and Bregs were significantly increased in PLG-PIO, PLGA-exo and PLGA-exo-PIO treatment groups when compared to PC group. In contrast, the frequencies of proinflammatory cells ($IL\text{-}4^+CD4^+$) were decreased from 6.90 ± 2.29 in PC group to 2.08 ± 0.58 in PLGA-exo-PIO group (Fig. 8E). Subsequently, the whole blood cells were also stained with CCR3 to gate the frequencies of eosinophils and basophils, and with CD63 and FcεRI to detect the degranulation of basophils after final treatment. As demonstrated in Fig. 8F, the $CCR3^+$ cell population was 1.35 ± 0.31, 8.06 ± 2.94, 8.11 ± 2.43, 6.41 ± 1.36, 4.38 ± 0.29, and 2.19 ± 0.18 in NC, PC, Blank PLGA, PLGA-PIO, PLGA-exo, PLGA-exo-PIO groups, suggesting that intranasal administration of PLGA-exo-PIO is capable to reduce the infiltration of eosinophils in AR + asthma mice. Finally, the flow cytometric analysis revealed that PLGA-exo-PIO treatment leads to significantly decreased degranulation of basophils in OVA-induced AR + asthma mice. The representative histograms of basophils are shown in Fig. 8G and H. From these results, we conclude that intranasal inoculation of PLGA-exo-PIO could significantly modulate the inflammatory cells and cytokines in vivo.

PLGA-exo-PIO treatment modulates the inflammatory cells and factors in the Bronchoalveolar lavage fluid of AR and asthma mice

It was further evaluated whether administering PLGA-exo-PIO can suppress the inflammatory cells and factors in the BALF of OVA-induced allergic mice. The total number of cells, eosinophils, and neutrophils in the BALF were counted for each treatment group after the final inoculation. We found that the BLAF of PLGA-PIO, PLGA-exo, and PLGA-exo-PIO treated mice possessed significantly lower numbers of total cells, eosinophils, and neutrophils compared with PC and Blank PLGA treated groups (Fig. 7A). The BALF supernatant exhibited a marked reduction of histamine, sIgE, IL-4, and IL-17 and elevation of IFN-γ, and IL-10 cytokines when PLGA-exo-PIO treated group was compared with model group (PC) (Fig. 7B). Additionally, results of flow cytometry showed the presence of 2.27 ± 0.84, 6.53 ± 2.13, 7.92 ± 3.19, 5.46 ± 1.68, 3.75 ± 1.07, and 2.14 ± 0.26% of $CD45^+CD170^+CD11c^-$ cells in NC, PC, Blank PLGA, PLGA-PIO, PLGA-exo and PLGA-exo-PIO groups, respectively in BALF, indicating the significant reduction of eosinophils after treatment (Fig. 7C). These data collectively proved the excellent in vivo anti-inflammatory ability of PLGA-exo-PIO nanocarriers and also signify

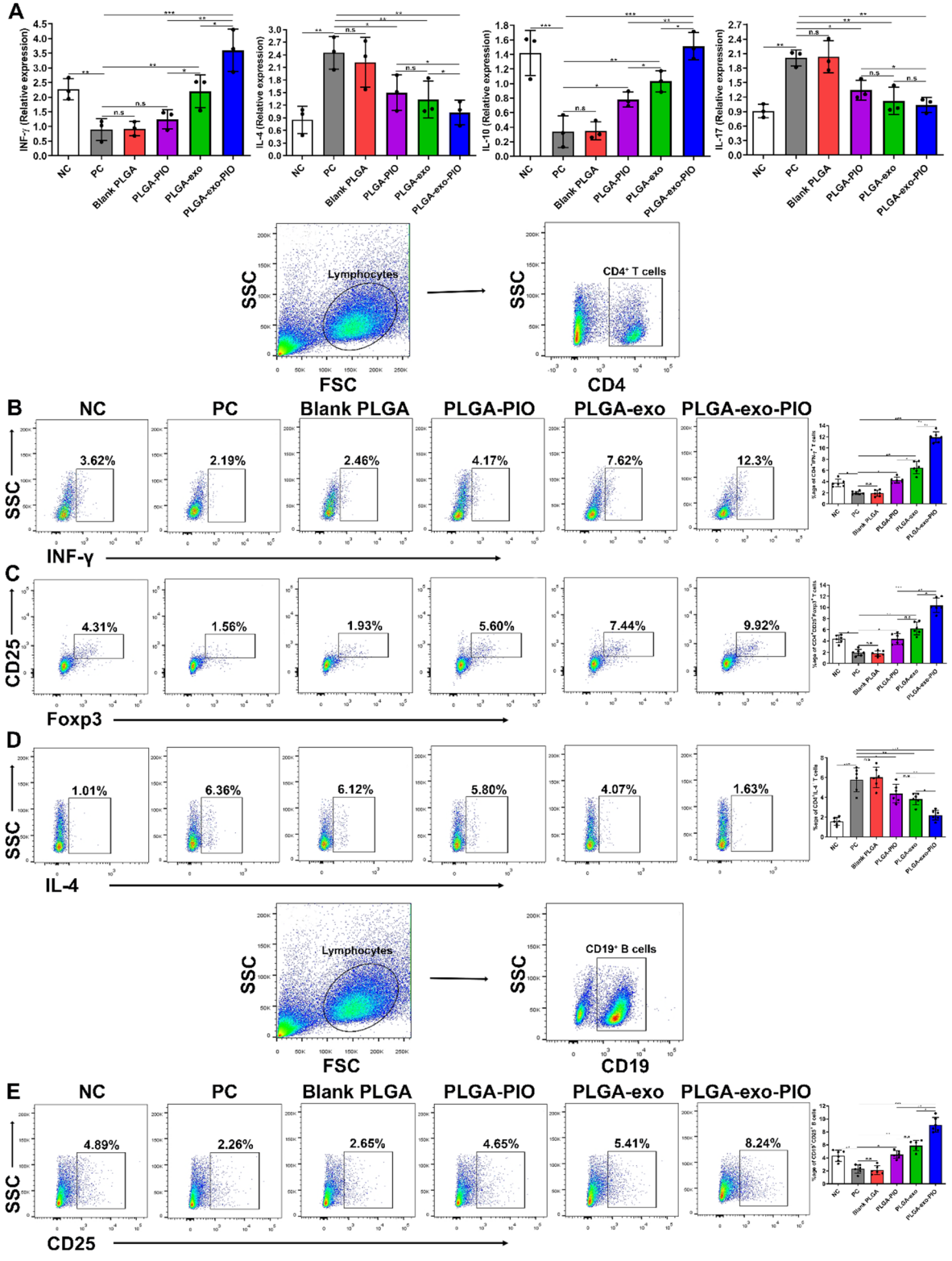

Fig. 7 PLGA-exo-PIO treatment exerts anti-inflammatory effects both at genetic and cellular levels in the spleen of AR and asthma mice. (**A**) Relative expression of mRNA for IFN-γ, IL-4, IL-10, and IL-17 in the spleen of AR + asthma mice. The frequencies of (**B**) $CD4^+IFN\text{-}\gamma^+$, (**C**) $CD4^+CD25^+Foxp3^+$, (**D**) $CD4^+IL\text{-}4^+$ T cells, and (**E**) $CD19^+CD25^+$ B cells in the spleen of AR + asthma mice. ($n = 6$ in each group, n.s = not significant, $^*p < 0.05$, $^{**}p < 0.01$, $^{***}p < 0.001$)

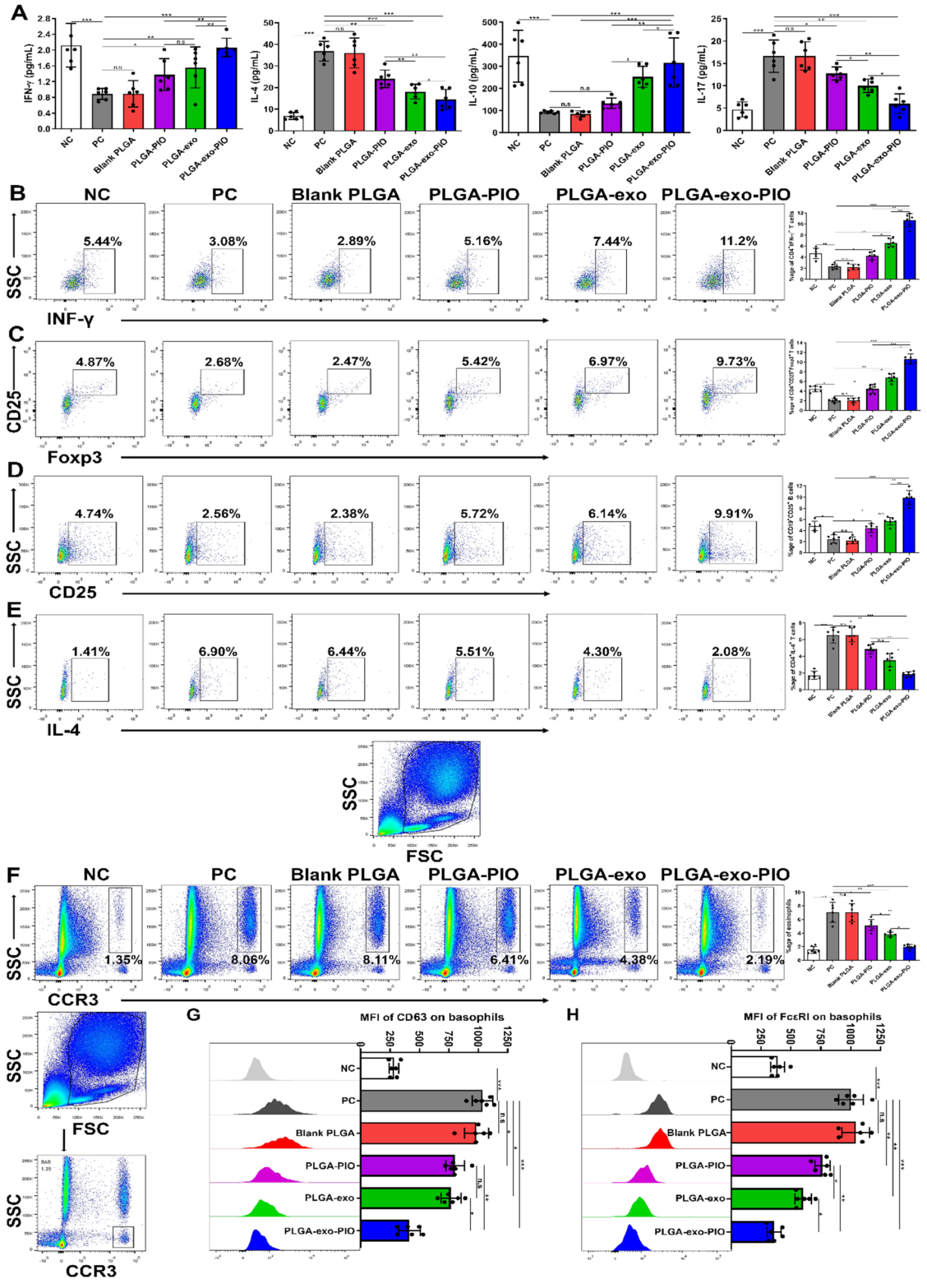

Fig. 8 PLGA-exo-PIO treatment reduces the inflammatory cells and cytokines in the blood of AR and asthma mice. (**A**) The concentrations of IFN-γ, IL-4, IL-10, and IL-17 in the serum. The frequencies of (**B**) $CD4^+IFN\text{-}\gamma^+$, (**C**) $CD4^+CD25^+Foxp3^+$ T cells, (**D**) $CD19^+CD25^+$ B cells, and (**E**) $CD4^+IL\text{-}4^+$, T cells in PBMCs. Percentage of (**F**) eosinophils, (**G**) $CD63^+$, and (**H**) $Fc\varepsilon RI^+$ basophils in whole blood of AR + asthma mice. ($n = 6$ in each group, n.s = not significant, $^*p < 0.05$, $^{**}p < 0.01$, $^{***}p < 0.001$)

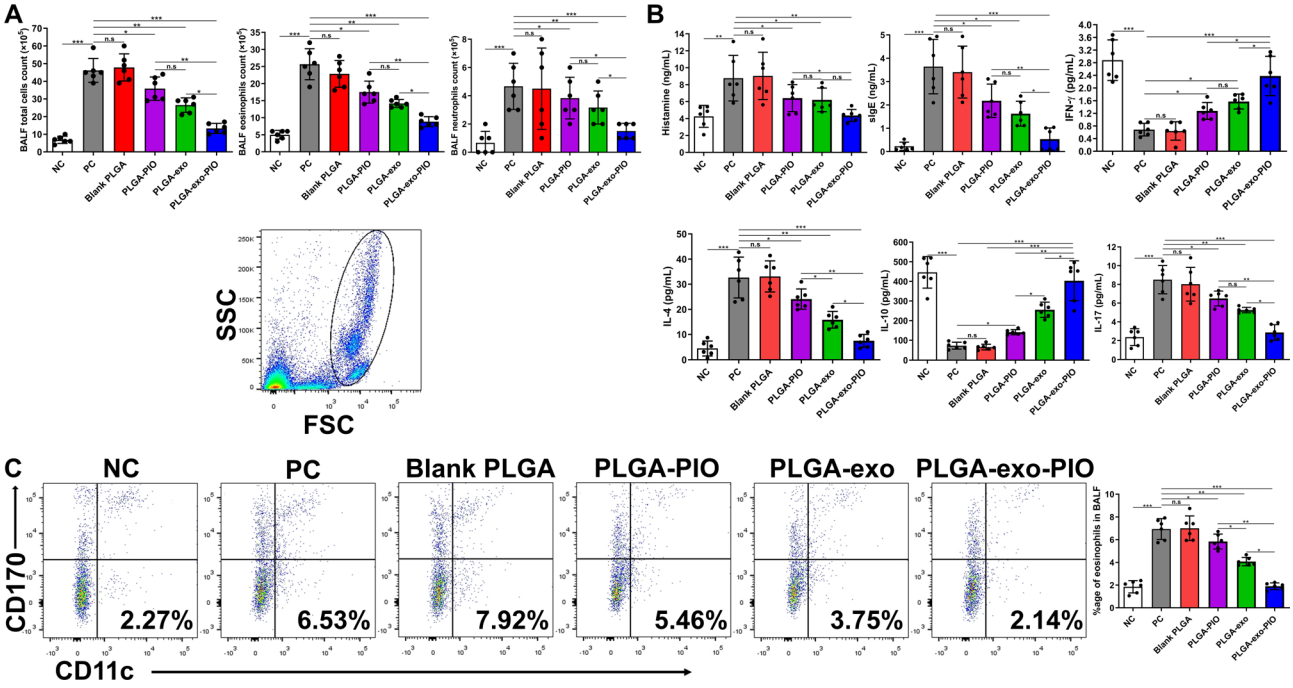

Fig. 9 PLGA-exo-PIO treatment modulates the inflammatory cells and factors in BALF of AR and asthma mice. (**A**) Total cells, eosinophils, and neutrophils count in BALF after wright's staining. (**B**) The concentrations of histamine, sIgE, IFN-γ, IL-4, IL-10, and IL-17 in the BALF. (**C**) The frequencies of $CD45^{+}CD170^{+}CD11c^{-}$ eosinophils in the BALF of AR + asthma mice. ($n = 6$ in each group, n.s = not significant, $^{*}p < 0.05$, $^{**}p < 0.01$, $^{***}p < 0.001$)

the importance of exosomes and PPAR-γ agonist to modulate the inflammatory responses.

To assess whether intranasal delivery of PLGA-exo-PIO causes any side effect in recipient mice, histopathological analysis was performed for vital organs (lungs, liver, kidney, heart and spleen) using H&E staining. No apparent organ toxicity was observed among all treatment groups (Fig. S5A). Additionally, no obvious change in serum biomarkers for liver and kidney functions was noted (Figs. S5B & C). Finally, routine blood tests of different treatment groups also presented no significant change in important parameters in full blood count (Fig. S5D). These data highlighted intranasal administration of PLGA-exo-PIO mediates safe, highly efficient cargo delivery and achieves targeted immunotherapy in vivo.

Bioinformatic trend analysis revealed consistent functional changes during RNA sequencing of nasal tissue and lung tissue

After collecting nasal and lung tissues from the NC, PC, and PLGA-exo-PIO groups, we performed bulk-RNA sequencing and detected similar trends in RNA transcription (Figs. 5A **& B**). Upon comparing nasal and lung tissue, our sequencing results showed upregulation of leukocyte migration, response to chemokine, and oxidative stress-related GO terms genes in AR and asthma mice before treatment. After treatment, the genes of GO terms related to neurotransmitter transport were universally upregulated in the PLGA-exo-PIO group, partially elucidating PLGA-exo-PIO's therapeutic effects on AR and asthma. Venn diagrams showed that after treatment, several genes were consistently upregulated in cilium organization and microtubule bundle formation in the nasal and lung tissues (Fig. 5C), while genes in immunoglobulin-mediated immune response and cytokine-mediated signaling pathway were down-regulated in NT and LT of treatment groups (Fig. 5D). These up- and down-regulated GO-enriched nodes were further analyzed (Figs. S6A-F) demonstrating specific therapeutic effect of PLGA-exo-PIO in aspects such as functional enhancement of respiratory epithelium and suppression of inflammation.

Focusing on up-regulated enrichment nodes in PLGA-exo-PIO group, bar graphs showed GO enrichment secondary functions of up-regulated genes (Fig. 5E). Enrichment circle plots and network diagrams showed upregulated genes focusing on cilium organization, cilium assembly, microtubule bundle formation entries (Figs. 5F, S6G). Hierarchical clustering of enriched terms performed by treeplot dendrograms revealed that PLGA-exo-PIO improved the function of cilium assembly basal body and postsynaptic active membrane zone (Fig. 5G). In contrast, up-regulated genes in the PC group were enriched for biological functions such as immunoglobulin-mediated immune response, lymphocyte-mediated immunity, tumor necrosis factor superfamily cytokine production function, and clustered in complement chemokine activation biotic, tumor necrosis factor cytokine,

and adaptive mediated immunity immunoglobulin (Figs. S6H-J). Together, the data from RNA sequencing of NT and LT showed consistent alterations in biological functions, thereby exploring the molecular mechanism of the therapeutic potential of PLGA-exo-PIO for united airway diseases.

Bioinformatic enrichment analysis focused on the effector signaling pathways of PLGA-exo-PIO treatment of AR and asthma

The volcano plots showed differentially expressed genes (DEGs) between pre-treatment (AR + asthma mice) and post-treatment (PLGA-exo-PIO) in the nasal tissue and lung tissue (Figs. 6A **& B**). KEGG enrichment analysis was performed to reveal the potential mechanism of PLGA-exo-PIO treatment (Fig. 6C and D). We found that fatty acid metabolism, axon guidance, and the PPAR signaling pathway were upregulated in the nasal tissue, and the leukocyte migration, TNF signaling pathway, and C-type lectin receptor signaling pathway were downregulated (Figs. 6C, S7A & S7B). In the lung tissue, PI3K-Akt signaling pathway, asthma-related pathway, and phospholipase D signaling pathway were upregulated, while the NF-kappa B signaling pathway, IL-17 signaling pathway, TNF signaling pathway, and C-type lectin receptor signaling pathway were downregulated (Figs. 6D, S7C & S7D). Collectively, these results suggested that PLGA-exo-PIO treatment shares common signaling pathway characteristics in AR and asthma. Further in-depth verification using GSEA (Figs. S7E & S7F) revealed few positive regulatory pathways, such as olfactory transduction, the Notch signaling pathway, and neuroactive ligand-receptor interaction, may play a potent role in the PLGA-exo-PIO treatment (Figs. 6E, F, I **& J**). In addition, several negative regulatory pathways, including cytokine-cytokine receptor interaction, oxidative phosphorylation, and complement and coagulation cascades (Figs. 6G, H, K **& L**), may explain the changes in immune cell and cytokine profiles after PLGA-exo-PIO treatment. *TNFAIP3*, *PTGS2*, *IL-6*, and *CXCL2* genes were significantly upregulated in the NF-κB pathway, whereas *CDKN1A* gene was downregulated, and *GATA3*, *Notch 4*, and *MFNG* genes were upregulated in the Notch pathway. A heatmap of key genes that were significantly upregulated or downregulated NF-κB and Notch pathways are presented in Fig. S8.

Discussion

Our findings support that both MSC-exo alone and its PIO-supplemented counterpart could serve as an effective therapy for allergic respiratory diseases. Firstly, stem cell-derived exosome therapy might be superior to stem cell therapy, as it avoids inevitable limitations such as infusion toxicity, immunogenicity, tumorigenic potentials, and ethical issues [35]. Exosomes have been regarded as miniature versions of their parental cells, partially because exosomes from a certain cell type carry cell-specific or unique sets of biomolecules [36]. For example, the MSC-derived exosomes used in our study, irrespective of the modality of their delivery, have successfully demonstrated anti-inflammatory and immunomodulatory effects in a preclinical model without exhibiting the disadvantages their cellular counterparts present. Secondly, although MSC-exo has been preclinically used in the treatment of respiratory diseases such as acute respiratory distress syndrome, chronic obstructive pulmonary disease and COVID-19 [14], much less evidence is available in airway inflammatory disorders such as AR or asthma. Yu et al. [37] and Tan et al. [16] used human adipose tissue and umbilical cord as tissue source for MSC-exo treatment of AR, respectively. Du et al. demonstrated a similar immunosuppressive effect on Tregs in asthma [38]. However, these studies were all single disease-oriented and none of them focused on AR and asthma as UADs. Lastly, in our very recent study in stem cell-derived exosomal therapy for rhinitis [16], multiomic analysis identified the PPAR pathway as a major molecular mechanism. PPARs, including PPAR-α, PPAR-β/δ, and PPAR-γ, are a family of ligand-activated transcription factors [39]' [40]. The therapeutic potential of PPAR-γ agonists for negative regulation of mast cell maturation, attenuation of inflammation in allergic airway disease, and remodeling of mucus hypersecretion have been reported [40, 41]. Future research could adopt other exosome-based drug delivery and tissue targeting as novel strategies to strengthen the therapeutic effects of MSC-exo [20, 42, 43].

Our findings support that PLGA nanoparticles could not only efficiently encapsulate exosomes but also sustainably deliver them in the nasal cavities and lungs. Firstly, compared to systemic venous administration, local delivery of exosomes might provide a prolonged therapeutic effect. In terms of MSC-exo treatment of AR, Yu's team delivered exosomes through tail vein injection which might face rapid clearance [44], whereas Tan's team did so using PLGA encapsulation which facilitated intranasal retention longer than 96 h [16, 37]. Based on our last project, current work extended PLGA-facilitated local exosome delivery from nasal cavity to lungs, thereby covering almost the entire respiratory tract. Another potential advantage of PLGA over venous delivery is that it might reduce the number of exosomes needed to reach the same degree of therapeutic effect. Secondly, the choice of biomaterials used for local delivery of exosomes depends on the pathological context [24]. In terms of airway delivery, several crucial properties support PLGA particles as an ideal platform for immunotherapy, such as FDA and EMA approval for mucosal and parental

administrations, complete degradation, minimal toxicity, high bioavailability, and controlled release of loaded cargo [45]. As a result, PLGA-based micro/nanoparticles have been exploited as promising delivery vehicles for the treatment of respiratory diseases [46]. However, we are the first to use PLGA nanoparticles in multiple airway diseases simultaneously. Lastly, as one of the key advantages of PLGA system, drug loadability and modifiability make them suitable for the delivery of various drugs such as corticosteroids (e.g., dexamethasone), neurotrophins (e.g., brain-derived neurotrophic factor), and anti-cancer medications (e.g., oxaliplatin) [47]. In addition, André et al. adopted a combined approach using cell and drug delivery [48]. For the first time, we used PLGA nanoparticles to load both medication and cell-derived exosomes. Future work could focus on optimizing the synthesis method for cargo-loaded PLGA micro/nanoparticles toward an improved delivery [49].

Our findings support that both upper and lower airway diseases in the same individual could be managed using PIO-supplemented MSC-exo. Firstly, conventional therapies for UADs possess inevitable limitations. Although corticosteroids and leukotriene receptor antagonists could provide symptomatic relief, their administration might be complicated (e.g., intranasal spray for AR and inhalation for asthma) and thus laborious for the patients. On the other hand, although allergen immunotherapy might be more radical than pharmacotherapy, it is time-consuming and might elicit life-threatening anaphylaxis [50]. Our single-modality approach proved to be simplified, rapid, and safe for anatomical units at two different locations. Secondly, PLGA-exo-PIO treatment could regulate the Th1/Th2 balance while affecting both Tregs and Bregs. Both types of regulatory cells secrete IL-10, reduce Th2 cells, and inhibit IgE production, thereby contributing to the pathogenesis of and treatment response in allergic asthma and rhinitis [51, 52]. However, most previous studies focused on the role of Tregs while underinvestigating that of Bregs. Our pharmaco-exosomal therapy could significantly boost the numbers of Tregs and Bregs, which might have a deeper impact on the mechanistic exploration of UADs. Lastly, PLGA-exo-PIO treatment could suppress the production of both eosinophils and basophils. The contemporary concept of allergy is a group of IgE-mediated diseases. However, recent theory support activated mast cells and/or basophils, other than IgE, also as mediators in sensitive patients of AR and asthma [53]. This might help explain why newer therapy such as Omalizumab, a monoclonal anti-IgE antibody, infrequently proves ineffective in severe patients [54]. The current study is the first to investigate the change of basophils in murine peripheral blood after exosomal treatment, which helps elucidate its cellular mechanism.

Our bioinformatic analyses revealed overlapping molecular changes in both nasal and lung tissues after the pharmaco-exosomal therapy. Firstly, the molecular profile after sequencing appeared to be treatment-specific and disease-specific [55]. For example, KEGG enrichment analysis in our recent study of MSC-exo treatment of rhinitis revealed few potentially crucial signaling pathways such as the PPAR pathway, glycolysis pathway and AMPK pathway [16]. In comparison, our current study of MSC-exo-PIO treatment of AR and asthma discovered several signaling cascades that are simultaneously affected in both nasal and lung tissues, such as the downregulated NF-κB pathway and TNF pathway. Secondly, the Notch pathway, as discovered in GSEA analysis, is worth further discussion and verification. The Notch cascade is an evolutionarily conserved pathway that coordinates juxtracrine cellular signaling by which a wide range of cell fate decisions in cardiac, neuronal, and immune systems are determined [56]. More importantly, the Notch pathway is implicated in both acute allergic airway inflammation and chronic airway remodeling. For example, antigen-presenting cells used the Notch pathway to instruct T cell differentiation with Notch ligand-specific fates [57], whereas Tregs inhibit sprouting angiogenesis of the airway remodeling by the Notch signaling, thereby leading to improved lung function [58]. Therefore, manipulating the Notch pathway might be one of the crucial molecular mechanisms of our novel pharmaco-exosomal therapy of UADs. Future work in exosome-based airway therapy could focus on the engineering of the exosomes using Notch agonists.

These improvements enable the PLGA-based drug delivery system with promising therapeutic effects on allergic airway diseases; however, its implications for humans still have some limitations. Additionally, before clinical trials, the donor of MSCs should be investigated for infectious or genetic diseases. In our study, we intranasally administered exosomes at a dose of 3.2×10^8 particles/mL, which was effective and safe in mice. Recent human clinical trials have proved that the concentration from 1.7×10^8 to 4.2×10^{15} particles/mL per kg of administered exosomes through different routes was therapeutically effective and safe [59–61]. The concentration of exosomes in humans needs to be calculated using the human-equivalent dose (HED), a standard allometric scaling method. This also theoretically suggests that our exosomes are safe for treatment in the human body. The heterogenicity of MSC-derived exosomes is a great challenge. A rigorous quality control system of exosomes is critical to reduce batch-to-batch variation. To tackle these challenges, recently, GMP grade MSCs [62, 63] derived from pluripotent stem cells have been proposed as an alternative source [64, 65] for EVs products. Additionally, the acquisition of exosomes requires a large

amount of cellular secretion for extraction, which might increase the treatment cost of exosomal therapy. Further studies are needed to explore the exact signaling pathways, the potential immunogenicity of repeated intranasal nanoparticle/exosome administration in humans, and the dosage of exosomes for clinical use.

Conclusions

We are the first group to develop a novel pharmaco-exosomal immunotherapy for united airway diseases. Firstly, MSC-derived exosomes supplemented by PPAR-γ agonist could exert anti-inflammatory effect for both allergic rhinitis and asthma in the same individual. Secondly, PLGA nanoparticles could act as a suitable vehicle for local and sustained delivery of exosomes for upper and lower airways. Thirdly, mechanistic exploration of PLGA-exo-PIO treatment revealed multiple signaling pathways such as the Notch cascade and NF-κB cascade. In conclusion, our work provides great potential in designing future personalized treatment for patients with synchronous diseases affecting both upper and lower respiratory tracts.

Abbreviations

AR	Allergic rhinitis
HNEpCs	Human nasal epithelial cells
IgE	Immunoglobulin E
IL	Interleukin
LPS	Lipopolysaccharide
LTC4	Leukotriene C4
LT	Lung tissue
MSCs	Mesenchymal stem cells
NTA	Nanoparticle tracking analysis
NT	Nasal tissue
PPAR-γ	Peroxisome proliferator-activated receptor gamma
PLGA	Poly(lactic-co-glycolic acid)
PIO	Pioglitazone
SIT	Specific immunotherapy
TEM	Transmission electron microscopy
Th2	T helper 2 cell
TNF	Tumor necrosis factor
Tregs	Regulatory T cells
UADs	United airway diseases

Supplementary Information

The online version contains supplementary material available at https://doi.org/10.1186/s13287-025-04624-8.

Supplementary Material 1

Acknowledgements

The authors used BioRender software (https://www.biorender.com/) to draw the graphical abstract of this manuscript.

Author contributions

K.A.S, and Z.W contributed equally to this work. K.A.S, Z.W and F.T designed this study. K.A.S, Z.W, B.C, and Xiaohui.L performed the experiments. K.A.S and Z.W performed experiment for supplementary data at revision stage. K.A.S, Z.W, B.C, and Y.W analyzed the data. Xuran.L helped with maintenance. K.A.S, F.T, B.C, and W.Z wrote the manuscript. F.T supervised the whole project. All authors read and approved the manuscript.

Funding

The present study was financially supported by Fundamental Research Funds for Central Universities and National Natural Science Foundation of China (No. 82271192) and the Subject Assistance Program of Shanghai Fourth People's Hospital (SY-XKZT-2023-1002 and SY-XKZT-2024-1012).

Data availability

All data generated and analyzed in this study are included in the article.

Data availability

The datasets generated and analyzed during the current study are available in the Sequence Read Archive (SRA) of the National Center for Biotechnology Information (NCBI) public database repository with BioProject accession No. PRJNA1148344, (https://www.ncbi.nlm.nih.gov/sra/PRJNA1148344).

Declarations

Ethics approval and consent to participate

Animal experiments executed in this study were approved as the "Therapeutic effect of PPAR-γ agonists decorated PLGA encapsulated MSC-exosomes to cure allergic rhinitis and asthma" by the ethical committee of the School of Medicine, Tongji University (approval no. TJ-HB-LAL-2024-29) on "2024-07-03" and performed following the recommendations of the Guide for Care and Use of Laboratory Animals of the Ministry of Science and Technology of People's Republic of China. Procell Life Science & Technology, Co., Ltd. has confirmed that there was initial ethical approval for the collection of mast and Human nasal epithelial cells (HNEpCs) and the donors had signed the informed consent. Whereas, for human umbilical cord-derived mesenchymal stem cells (HUC-MSCs), Cytoniche Biotechnology Co., Ltd. has confirmed that there was initial ethical approval for the collection of human cells and the donors had signed the informed consent.

Consent for publication

All authors agree to the publication of this work.

Competing interests

All the authors declare that they have no conflict of interest.

Use of AI

The authors declare that they have not used AI-generated work in this manuscript.

Author details

[1]Department of ORL-HNS, Shanghai Fourth People's Hospital, and School of Medicine, Tongji University, Shanghai, China
[2]Plasma Medicine and Surgical Implants Center, Tongji University, Shanghai, China
[3]Department of Respiratory and Critical Care Medicine, Shanghai Fourth People's Hospital, Tongji University School of Medicine, Shanghai, China
[4]The Royal College of Surgeons in Ireland, Dublin, Ireland
[5]The Royal College of Surgeons of England, London, UK

Received: 15 May 2025 / Accepted: 21 August 2025
Published online: 02 September 2025

References

1. Jiang J, Mehrabi Nasab E, Athari SM, Athari SS. Effects of vitamin E and selenium on allergic rhinitis and asthma pathophysiology. Respir Physiol Neurobiol. 2021;286:103614.
2. Bergantini L, Cameli P, d'Alessandro M, Vietri L, Perruzza M, Pieroni M, et al. Regulatory T cells in severe persistent asthma in the era of monoclonal antibodies target therapies. Inflammation. 2020;43:393–400.
3. Arshad SH. Does allergen immunotherapy for allergic rhinitis prevent asthma? Ann Allergy Asthma Immunol. 2022;129:286–91.
4. Bardin PG, Holmes PW, Hamilton G. Exploring united airways. Respirology. 2013;18:893–4.
5. Holgate ST. Innate and adaptive immune responses in asthma. Nat Med. 2012;18:673–83.

6. Brusselle GG, Maes T, Bracke KR. Eosinophils in the spotlight: eosinophilic airway inflammation in nonallergic asthma. Nat Med. 2013;19:977–9.
7. Wisniewski JA, Muehling LM, Eccles JD, Capaldo BJ, Agrawal R, Shirley DA et al. T(H)1 signatures are present in the lower airways of children with severe asthma, regardless of allergic status. J Allergy Clin Immunol. 2018;141:2048-60.e13.
8. Shahzad KA, Wang Z, Li X, Li J, Xu M, Tan F. Immunomodulatory effect of PLGA-encapsulated mesenchymal stem cells-derived exosomes for the treatment of allergic rhinitis. Front Immunol. 2024;15.
9. Jang TY, Park CS, Kim KS, Heo MJ, Kim YH. Benzaldehyde suppresses murine allergic asthma and rhinitis. Int Immunopharmacol. 2014;22:444–50.
10. Lee H, Ryu J, Nam E, Chung SJ, Yeo Y, Park DW et al. Increased mortality in patients with corticosteroid-dependent asthma: a nationwide population-based study. Eur Respir J. 2019;54.
11. Hoang DM, Pham PT, Bach TQ, Ngo ATL, Nguyen QT, Phan TTK, et al. Stem cell-based therapy for human diseases. Signal Transduct Target Ther. 2022;7:272.
12. Lou G, Chen Z, Zheng M, Liu Y. Mesenchymal stem cell-derived exosomes as a new therapeutic strategy for liver diseases. Exp Mol Med. 2017;49:e346.
13. Zhang K, Cheng K. Stem cell-derived exosome versus stem cell therapy. Nat Reviews Bioeng. 2023.
14. Zargar MJ, Kaviani S, Vasei M, Soufi Zomorrod M, Heidari Keshel S, Soleimani M. Therapeutic role of mesenchymal stem cell-derived exosomes in respiratory disease. Stem Cell Res Ther. 2022;13:194.
15. Hong D, Hu Z, Weng J, Yang L, Xiong Y, Liu Y. Effect of mesenchymal stem cell therapy in animal models of allergic rhinitis: A systematic review and meta-analysis. Int Immunopharmacol. 2023;124:111003.
16. Shahzad KA, Wang Z, Li X, Li J, Xu M, Tan F. Immunomodulatory effect of PLGA-encapsulated mesenchymal stem cells-derived exosomes for the treatment of allergic rhinitis. Front Immunol. 2024;15:1429442.
17. Liu W, Ota M, Tabushi M, Takahashi Y, Takakura Y. Development of allergic rhinitis immunotherapy using antigen-loaded small extracellular vesicles. J Control Release. 2022;345:433–42.
18. Wu J, Huang QM, Liu Y, Zhou J, Tang WR, Wang XY, et al. Long-term hypoxic hUCMSCs-derived extracellular vesicles alleviates allergic rhinitis through triggering immunotolerance of their VEGF-mediated Inhibition of dendritic cells maturation. Int Immunopharmacol. 2023;124:110875.
19. Zhao C, Wei X, Kong W, Zhao Y, Yang J, Cheng J, et al. Mesenchymal stem cell derived extracellular vesicles loaded thermosensitive chitosan-based hydrogel alleviates allergic rhinitis in mouse model. Mater Design. 2023;233:112271.
20. Zhang Y, Bi J, Huang J, Tang Y, Du S, Li P, Exosome. A review of its classification, isolation techniques, storage, diagnostic and targeted therapy applications. Int J Nanomed. 2020;15:6917–34.
21. Smyth T, Kullberg M, Malik N, Smith-Jones P, Graner MW, Anchordoquy TJ. Biodistribution and delivery efficiency of unmodified tumor-derived exosomes. J Control Release. 2015;199:145–55.
22. Betzer O, Perets N, Angel A, Motiei M, Sadan T, Yadid G, et al. Vivo neuroimaging of exosomes using gold nanoparticles. ACS Nano. 2017;11:10883–93.
23. Han Y, Zhu Y, Youngblood HA, Almuntashiri S, Jones TW, Wang X, et al. Nebulization of extracellular vesicles: A promising small RNA delivery approach for lung diseases. J Control Release. 2022;352:556–69.
24. Tan F, Xu M, Li X, Wang Z, Li J, Shahzad KA. Biomaterial-Facilitated local delivery of stem Cell-Derived small extracellular vesicles: perspectives in surgical therapy. Adv Ther. 2024;n/a:2300387.
25. Khayambashi P, Iyer J, Pillai S, Upadhyay A, Zhang Y, Tran SD. Hydrogel encapsulation of mesenchymal stem cells and their derived exosomes for tissue engineering. Int J Mol Sci. 2021;22.
26. Shahzad KA, Wan X, Zhang L, Pei W, Zhang A, Younis M, et al. On-target and direct modulation of alloreactive T cells by a nanoparticle carrying MHC alloantigen, regulatory molecules and CD47 in a murine model of alloskin transplantation. Drug Deliv. 2018;25:703–15.
27. Wan X, Pei W, Shahzad KA, Zhang L, Song S, Jin X, et al. Correction: A tolerogenic artificial APC durably ameliorates experimental autoimmune encephalomyelitis by directly and selectively modulating Myelin Peptide-Autoreactive CD4(+) and CD8(+) T cells. J Immunol. 2020;204:728–9.
28. Shen DD, Pang JR, Bi YP, Zhao LF, Li YR, Zhao LJ, et al. LSD1 deletion decreases Exosomal PD-L1 and restores T-cell response in gastric cancer. Mol Cancer. 2022;21:75.
29. Zhu X, Wang X, Wang Y, Zhao Y. Exosomal long non-coding RNA GAS5 suppresses Th1 differentiation and promotes Th2 differentiation via downregulating EZH2 and T-bet in allergic rhinitis. Mol Immunol. 2020;118:30–9.
30. Morales-Kastresana A, Jones JC. Flow cytometric analysis of extracellular vesicles. Methods Mol Biol. 2017;1545:215–25.
31. González-Cubero E, González-Fernández ML, Gutiérrez-Velasco L, Navarro-Ramírez E, Villar-Suárez V. Isolation and characterization of exosomes from adipose tissue-derived mesenchymal stem cells. J Anat. 2021;238:1203–17.
32. Sah AK, Suresh PK, Verma VK. PLGA nanoparticles for ocular delivery of Loteprednol etabonate: a corneal penetration study. Artif Cells Nanomed Biotechnol. 2017;45:1–9.
33. Dong L, Wang Y, Zheng T, Pu Y, Ma Y, Qi X, et al. Hypoxic hUCMSC-derived extracellular vesicles attenuate allergic airway inflammation and airway remodeling in chronic asthma mice. Stem Cell Res Ther. 2021;12:4.
34. Mikhak Z, Fukui M, Farsidjani A, Medoff BD, Tager AM, Luster AD. Contribution of CCR4 and CCR8 to antigen-specific T(H)2 cell trafficking in allergic pulmonary inflammation. J Allergy Clin Immunol. 2009;123:67–e733.
35. Zakrzewski W, Dobrzynski M, Szymonowicz M, Rybak Z. Stem cells: past, present, and future. Stem Cell Res Ther. 2019;10:68.
36. Ren K. Exosomes in perspective: a potential surrogate for stem cell therapy. Odontology. 2019;107:271–84.
37. Yang W, Pan Z, Zhang J, Wang L, Lai J, Zhou S, et al. Extracellular vesicles from adipose stem cells ameliorate allergic rhinitis in mice by Immunomodulatory. Front Immunol. 2023;14:1302336.
38. Du YM, Zhuansun YX, Chen R, Lin L, Lin Y, Li JG. Mesenchymal stem cell exosomes promote immunosuppression of regulatory T cells in asthma. Exp Cell Res. 2018;363:114–20.
39. Belvisi MG, Mitchell JA. Targeting PPAR receptors in the airway for the treatment of inflammatory lung disease. Br J Pharmacol. 2009;158:994–1003.
40. Zhang Y, Li X, Fang S, Zhu Z, Yao M, Ying L, et al. Peroxisome proliferator-activated receptor γ agonist suppresses mast cell maturation and induces apoptosis. Mol Med Rep. 2017;16:1793–800.
41. Lakshmi SP, Reddy AT, Banno A, Reddy RC. Airway epithelial cell peroxisome Proliferator-Activated receptor γ regulates inflammation and mucin expression in allergic airway disease. J Immunol. 2018;201:1775–83.
42. Galimberti D, Scarpini E. Pioglitazone for the treatment of alzheimer's disease. Expert Opin Investig Drugs. 2017;26:97–101.
43. Shao J, Zaro J, Shen Y. Advances in Exosome-Based drug delivery and tumor targeting: from tissue distribution to intracellular fate. Int J Nanomed. 2020;15:9355–71.
44. Liu X, Yang Y, Li Y, Niu X, Zhao B, Wang Y, et al. Integration of stem cell-derived exosomes with in situ hydrogel glue as a promising tissue patch for articular cartilage regeneration. Nanoscale. 2017;9:4430–8.
45. Horvath D, Basler M. PLGA particles in immunotherapy. Pharmaceutics. 2023;15.
46. Guo X, Zuo X, Zhou Z, Gu Y, Zheng H, Wang X et al. PLGA-Based micro/nanoparticles: an overview of their applications in respiratory diseases. Int J Mol Sci. 2023;24.
47. Loureiro JA, Pereira MC. PLGA based drug carrier and pharmaceutical applications: the most recent advances. Pharmaceutics. 2020;12.
48. Andre EM, Delcroix GJ, Kandalam S, Sindji L, Montero-Menei CN. A Combinatorial Cell and Drug Delivery Strategy for Huntington's Disease Using Pharmacologically Active Microcarriers and RNAi Neuronally-Committed Mesenchymal Stromal Cells. Pharmaceutics. 2019;11.
49. Todaro B, Moscardini A, Luin S, Pioglitazone-Loaded PLGA. Nanoparticles: towards the most reliable synthesis method. Int J Mol Sci. 2022;23.
50. Nolte H, Calderon MA, Bernstein DI, Roberts G, Azuma R, Juhl RG, et al. Anaphylaxis in clinical trials of Sublingual immunotherapy tablets. J Allergy Clin Immunol Pract. 2024;12:85–95. e4.
51. Kliem CV, Schaub B. The role of regulatory B cells in immune regulation and childhood allergic asthma. Mol Cell Pediatr. 2024;11:1.
52. Huang F, Yin JN, Wang HB, Liu SY, Li YN. Association of imbalance of effector T cells and regulatory cells with the severity of asthma and allergic rhinitis in children. Allergy Asthma Proc. 2017;38:70 – 7.
53. He SH, Zhang HY, Zeng XN, Chen D, Yang PC. Mast cells and basophils are essential for allergies: mechanisms of allergic inflammation and a proposed procedure for diagnosis. Acta Pharmacol Sin. 2013;34:1270–83.
54. Miyake K, Karasuyama H. Emerging roles of basophils in allergic inflammation. Allergol Int. 2017;66:382–91.
55. Xu X, Yin J, Yang Y, Liu H, Yu J, Luo X, et al. Advances in co-pathogenesis of the united airway diseases. Respir Med. 2024;225:107580.
56. Bray SJ. Notch signalling in context. Nat Rev Mol Cell Biol. 2016;17:722–35.
57. Amsen D, Blander JM, Lee GR, Tanigaki K, Honjo T, Flavell RA. Instruction of distinct CD4 T helper cell fates by different Notch ligands on antigen-presenting cells. Cell. 2004;117:515–26.

58. Huang MT, Chiu CJ, Chiang BL. Multi-Faceted Notch in allergic airway inflammation. Int J Mol Sci. 2019;20.
59. Gupta D, Zickler AM, El Andaloussi S. Dosing extracellular vesicles. Adv Drug Deliv Rev. 2021;178:113961.
60. Lotfy A, AboQuella NM, Wang H. Mesenchymal stromal/stem cell (MSC)-derived exosomes in clinical trials. Stem Cell Res Ther. 2023;14:66.
61. Gotoh S, Kawabori M, Fujimura M. Intranasal administration of stem cell-derived exosomes for central nervous system diseases. Neural Regen Res. 2024;19:1249–55.
62. Bloor AJC, Patel A, Griffin JE, Gilleece MH, Radia R, Yeung DT, et al. Production, safety and efficacy of iPSC-derived mesenchymal stromal cells in acute steroid-resistant graft versus host disease: a phase I, multicenter, open-label, dose-escalation study. Nat Med. 2020;26:1720–5.
63. Kou M, Huang L, Yang J, Chiang Z, Chen S, Liu J, et al. Mesenchymal stem cell-derived extracellular vesicles for Immunomodulation and regeneration: a next generation therapeutic tool? Cell Death Dis. 2022;13:580.
64. Ma CY, Zhai Y, Li CT, Liu J, Xu X, Chen H, et al. Translating mesenchymal stem cell and their exosome research into GMP compliant advanced therapy products: promises, problems and prospects. Med Res Rev. 2024;44:919–38.
65. Lian Q, Zhang Y, Zhang J, Zhang HK, Wu X, Zhang Y, et al. Functional mesenchymal stem cells derived from human induced pluripotent stem cells attenuate limb ischemia in mice. Circulation. 2010;121:1113–23.

Publisher's note